

Validity of quasilinear theory: refutations and new numerical confirmation

This article has been downloaded from IOPscience. Please scroll down to see the full text article.

2011 Plasma Phys. Control. Fusion 53 025012

(<http://iopscience.iop.org/0741-3335/53/2/025012>)

View [the table of contents for this issue](#), or go to the [journal homepage](#) for more

Download details:

IP Address: 194.214.217.17

The article was downloaded on 24/01/2011 at 10:29

Please note that [terms and conditions apply](#).

Validity of quasilinear theory: refutations and new numerical confirmation

Nicolas Besse¹, Yves Elskens², D F Escande² and Pierre Bertrand¹

¹ UMR 7198 CNRS-Nancy Universités, Université Henri Poincaré, Bd des Aiguillettes, BP 70239, FR-54506 Vandœuvre-lès-Nancy Cedex, France

² UMR 6633 CNRS-Université de Provence, Faculté de St Jérôme, Case 321, Av. Normandie Niemen, FR-13397 Marseille Cedex 20, France

E-mail: nicolas.besse@iecn.u-nancy.fr, yves.elskens@univ-provence.fr and dominique.escande@univ-provence.fr

Received 9 June 2010, in final form 18 October 2010

Published 7 January 2011

Online at stacks.iop.org/PPCF/53/025012

Abstract

The validity of quasilinear (QL) theory describing the weak warm beam–plasma instability has been a controversial topic for several decades. This issue is tackled anew, both analytically and by numerical simulations which benefit from the power of modern computers and from the development in the last decade of Vlasov codes endowed with both accuracy and weak numerical diffusion. Self-consistent numerical simulations within the Vlasov-wave description show that QL theory remains valid in the strong chaotic diffusion regime. However, there is a non-QL regime before saturation, which confirms previous analytical work and numerical simulation, but contradicts another analytical work. We show analytically the absence of mode coupling in the saturation regime of the instability where a plateau is present in the tail of the particle distribution function. This invalidates several analytical works trying to prove or to contradict the validity of QL theory in the strongly nonlinear regime of the weak warm beam–plasma instability.

(Some figures in this article are in colour only in the electronic version)

1. Introduction

Wave–particle interaction is an important phenomenon in plasma physics. It stands at the root of wave heating, of numerous instabilities, and of some regimes of anomalous transport in magnetically confined plasmas. Wave–particle interaction, described by Vlasov–Maxwell equations or ‘simply’ by one-dimensional Vlasov–Poisson equations, is already so complex that Landau damping was fully recognized only after its experimental discovery in 1964 [45], even though it was discovered on an analytical basis in 1946 [38]. As to nonlinear description, the situation is worse and has led to a controversy recalled below about the validity of the quasilinear (QL) equations for describing the saturation of the weak warm beam–plasma

instability. Furthermore, QL estimates are quite frequently used for modelling in different branches of plasma physics, such as laser–plasma interaction or magnetized plasma turbulence. Since the QL approximation is ubiquitous, in particular in kinetic or gyrokinetic descriptions, it is important to assess its validity at least for the simplest problem of kinetic turbulence, namely the saturation of the weak warm beam–plasma instability. We now sketch this problem (see [27] for an intuitive introduction and chapter 7 of [22] for a more exhaustive one).

1.1. Formulation of the problem

We consider a two-dimensional distribution function of particles in (x, v) space which is initially given for a one-dimensional spatially uniform beam–plasma system. This beam corresponds to a bump on the tail of the electron velocity distribution function. Langmuir waves are destabilized by the inversion of the electron population corresponding to the positive slope interval of the distribution. They first grow linearly, but when the electron dynamics becomes chaotic enough in their range of phase velocities, the bump is eroded and eventually a plateau in the distribution function builds up. Simultaneously, there is a transfer of momentum from the particles to the waves, generating a turbulent spectrum of Langmuir waves. This scenario was first predicted on a theoretical basis [17, 56] by considering the wave–particle interaction as perturbative and neglecting all mode couplings in the Vlasov equation, except for their effect on the space-averaged distribution function f . This led to the set of QL equations coupling $f(t, v)$ and the waves field power spectrum $\psi(t, v)$, which is related (see (20)) to the (k -density of the) Poynting vector of the waves electric field:

$$\partial_t f = \partial_v (D_{\text{QL}}(t, v) \partial_v f), \quad (1)$$

$$\partial_t \psi = 2\gamma_{\text{L}}(t, v) \psi, \quad (2)$$

where

$$\gamma_{\text{L}}(t, v) = \frac{\pi}{2} \frac{\eta}{1 + \eta} \frac{\omega_{\text{p}}^3}{k^2} \partial_v f(t, v) \quad (3)$$

is the Landau growth rate computed with the instantaneous velocity distribution, while

$$D_{\text{QL}}(t, v) = \pi \frac{\eta}{1 + \eta} \frac{\psi(t, v)}{k^2} \quad (4)$$

is the QL diffusion coefficient. In these formulae, ω_{p} is the plasma frequency, and $\eta = n_{\text{b}}/n_{\text{p}}$ denotes the ratio of the beam density n_{b} (the tail particle distribution function) to plasma density n_{p} (the bulk particle distribution function). Note that phase velocity v and wavenumber k are linked by $v = \omega/k$ and the Bohm–Gross dispersion relation $\mathcal{D}(k, \omega) = 0$, namely

$$\omega^2/\omega_{\text{p}}^2 = 1 + 3k^2\lambda_{\text{D}}^2, \quad (5)$$

with $k\lambda_{\text{D}} \ll 1$ where λ_{D} is the Debye length. We focus on one-dimensional dynamics with periodic boundary conditions, so that the wave spectrum is discrete.

1.2. Some controversial issues

Later on, the QL scenario was confirmed experimentally [51], but with poor accuracy for γ_{L} and D_{QL} in the saturation regime. However, the quasi-ballistic assumption underlying QL calculations is incorrect in the saturation regime [1], as is recalled now. If at time t_0 velocity diffuses with a diffusion coefficient D_{QL} assumed to be independent of time for the moment, a particle velocity and position are stochastic processes, for which we denote by $\langle \cdot \rangle$ the expectations with respect to the law of random noise. In particular, $\langle \Delta v^2 \rangle \simeq 2D_{\text{QL}}(t - t_0)$ with

$\Delta v(t) = v(t) - v(t_0)$. Consequently particle positions spread as $\langle k^2 \Delta x^2 \rangle = \frac{2}{3} k^2 D_{\text{QL}} (t - t_0)^3$ for $\Delta x(t) = \int_{t_0}^t \Delta v(\tau) d\tau$. Therefore, positions spread over a typical wavelength of the turbulent wave spectrum when $\langle k^2 \Delta x^2 \rangle \simeq 4\pi^2$, which occurs for a time $\sim t_0 + \tau_{\text{spread}}$ with $\tau_{\text{spread}} = (6\pi^2 k^{-2} D_{\text{QL}}^{-1})^{1/3} \simeq 4\tau_{\text{D}}$, where

$$\tau_{\text{D}} = (k^2 D_{\text{QL}})^{-1/3} \quad (6)$$

is called the Dupree time [18], its reciprocal being the resonance-broadening frequency.

In order to describe completely the classical regime, denoted regime L(inear) in this work, where the original QL approximation is valid, we need to introduce other time scales. Let Δv_{spec} be the phase velocity width of the wave spectrum and Δv_{φ} be the typical phase velocity mismatch between neighbouring waves. For a typical wave number k , we then define the wave autocorrelation time $\tau_{\text{ac}} = (k \Delta v_{\text{spec}})^{-1}$, namely the time needed for a resonant particle to resolve the finite frequency width of the wave spectrum, and the discretization time $\tau_{\text{discr}} = (k \Delta v_{\varphi})^{-1}$, namely the time it takes a resonant particle to resolve the separate Doppler frequencies of the modes. Particles released at time t_0 have their velocity spread Δv that grows linearly with time for t below $t_0 + \tau_{\text{ac}}$, and $\langle \Delta v^2 \rangle$ grows quadratically, since all waves act with an almost constant force on the particle orbit during this time interval. Therefore there is no diffusion. For time beyond τ_{discr} , the dynamics feels the discreteness of the wave spectrum, and the perturbative motion, if physically relevant because $\tau_{\text{spread}} \gg \tau_{\text{discr}}$, is no longer diffusive but may be quasi-periodic. We now define the dimensionless parameters

$$\mu = (\gamma_{\text{L}} \tau_{\text{D}})^{-1}, \quad K_{\text{D}} = \tau_{\text{ac}} / \tau_{\text{D}}, \quad \mathcal{B} = \tau_{\text{D}} / \tau_{\text{discr}}, \quad (7)$$

where K_{D} is called the Kubo number. For a small enough initial waves amplitude and a correspondingly small enough Δv_{φ} , the initial QL regime (regime L) is characterized by $\mu \ll 1$, $K_{\text{D}} \ll 1$ and $\mathcal{B} \ll 1$. The parameter \mathcal{B} is linked to the Chirikov resonance overlap parameter $s_{\text{ov}} = 2\Delta v_{\text{trap}} / \Delta v_{\varphi}$ by the relation $\mathcal{B} = 8\pi^{-1/3} s_{\text{ov}}^{-4/3}$ where Δv_{trap} is the typical trapping width of a wave. Thus $\mathcal{B} \ll 1$ means $s_{\text{ov}} \gg 1$. The condition $\mu \ll 1$ cannot be satisfied during the whole saturation regime of the beam–plasma instability since the plateau formation means ultimately a vanishing slope of $f(t, v)$ and vanishing $\gamma_{\text{L}}(t, v)$. Therefore there is a crossover to the strongly nonlinear regime $\mu \gg 1$. Indeed strong mode coupling is seen both numerically and experimentally (see [13, 16, 39, 42] and references therein). However, although the QL assumption ceases to hold, the central question about the validity of QL equations remains unsolved in the strong nonlinear regime, denoted SNL and characterized by $\mu \gg 1$, $K_{\text{D}} \ll 1$ and $\mathcal{B} \ll 1$.

From a theoretical point of view, the validity of QL theory was questioned by Adam *et al* [1] when accounting for nonlinear wave coupling. The importance of this coupling was denied by Galeev *et al* [36]. In 1983, Laval and Pesme predicted an increase in the growth rate and diffusion coefficient with respect to their QL values when μ increases [39], and claimed the inconsistency of QL theory due to mode coupling [40]. They proposed a model predicting a renormalization by a factor 2.2 of the QL growth rate and diffusion coefficient on the basis of a ‘turbulent trapping’ ansatz (derived from a clump-theory-like approach [19]) in the nonlinear regime $\mu \gg 1$ [41], an improved version of their previous claim [1]. Aimed at checking this prediction, a first experiment reached a weakly nonlinear regime where mode coupling was strong, but no renormalization was found [55]. The difficulty of dealing analytically with strongly nonlinear regimes of the Vlasov–Poisson system motivated a new mechanical approach, further encouraged by progress in the understanding of low-dimensional Hamiltonian chaos [22]. The experiment of Tsunoda *et al* [55] further fuelled the ongoing controversy which produced about 20 analytical, numerical and experimental works over two decades. In particular, Liang and Diamond [43, 44] stated the turbulent trapping model to be

inconsistent because momentum conservation is violated. They proposed a derivation of the QL equations in the $\mu \gg 1$ regime by using the theory of two-point correlation functions initially proposed by Boutros-Ghali and Dupree [12]. Shapiro and Sagdeev [52], investigating the four-wave coupling, asserted that QL theory works if the particle distribution function and the wave spectrum are averaged over a width in velocity defined by $\langle \Delta v^2 \rangle \simeq 2D_{\text{QL}}\tau_{\text{D}} = 2\Delta v_{\text{D}}^2$ where

$$\Delta v_{\text{D}} = (D_{\text{QL}}/k)^{1/3} = k/\tau_{\text{D}} \quad (8)$$

is called the Dupree width. References [22, 29] derived QL equations in the $\mu \gg 1$ regime, by extending the technique for the non-self-consistent case thanks to the slow effect of one particle on a given wave [29].

As yet no consensus has been reached [22, 42]. Experiments and numerical simulations have not yet described the strongly nonlinear regime in an accurate way but are compatible with weak renormalization effects in the intermediate (nonlinear) regime, denoted INL, where $\mu \gtrsim 1$, $K_{\text{D}} \ll 1$ and $\mathcal{B} \ll 1$ [13, 16, 37, 42]³.

1.3. Position of this work

The numerical part of this paper presents complete self-consistent simulations in the Vlasovian framework, starting from regime L to reach regime SNL by passing through regime INL. Before seeing whether self-consistent QL theory is still valid in regime SNL, let us understand why QL equations still hold in the case of non-self-consistent dynamics with wave spectra like those in regime SNL under some assumptions on the wave spectrum that we will describe further. To understand particle diffusion, it is useful to consider first the case of diffusion in a prescribed set of $M \gg 2$ Langmuir waves with random phases and a smooth amplitude spectrum as defined by the Hamiltonian

$$\mathcal{H}_{\text{nsc}}(t, x, v) = \frac{v^2}{2} - \sum_{m=1}^M A_m \cos(k_m x - \omega_m t + \varphi_m). \quad (9)$$

If the wave spectrum is broad, classical perturbation theory predicts [22, 28–31] $\langle \Delta v^2 \rangle = 2D_{\text{QL}}t$ and $\langle k^2 \Delta x^2 \rangle = \frac{2}{3}k^2 D_{\text{QL}}t^3$ for $\tau_{\text{ac}} \ll t \ll \tau_{\text{pert}} = \min(\tau_{\text{D}}, \tau_{\text{discr}})$ where the bracket notation denotes averages over the random phases φ_m . This calculation defines D_{QL} over a time scale where the spreading of orbits is negligible, and thus chaos is unimportant. Therefore, diffusion is due to the randomness of the field, not to the dynamical chaos: this diffusion is stochastic but not chaotic. Note that $\tau_{\text{spread}} \simeq 4\tau_{\text{D}}$ bounds the time over which the dependence of the orbits over M phases is small.

According to the value of the overlap parameter s_{ov} , several scenarios have been observed numerically for $t > \tau_{\text{pert}}$ [14, 22]. At small s_{ov} , i.e. for $\mathcal{B} \gg 1$, there is no large-scale chaos and the dynamics first feels the discreteness of the wave spectrum. For $t > \tau_{\text{discr}}$ this dynamics proves to be quasi-periodic and $\langle \Delta v^2 \rangle$ saturates; thus the motion is no longer diffusive, which confirms that the initial QL diffusion is not chaotic over large velocity scales. At large s_{ov} , i.e. for $\mathcal{B} \ll 1$, the dynamics feels first the chaotic spreading of the orbits. Then, for $t > \tau_{\text{spread}}$ the

³ Related work [46, 47] (see also references therein and the physically insightful, well-referenced introduction) by Mouhot and Villani, on Landau damping in a nonlinear context, has brought the long awaited mathematical proof of (nonlinear) Landau damping in infinite time with exponential decay, for any interaction not more singular than Coulomb or Newton, including the limit case. As a corollary, they obtain new stability results for homogeneous equilibria of the nonlinear Vlasov–Poisson equation, under analytic perturbations. In particular they show the convergence, in the weak topology in infinite time with exponential rate of convergence, of small enough analytic perturbations towards spatially homogeneous analytic equilibrium profiles which cannot be described in terms of conservation laws and initial datum alone.

dynamics remains diffusive with a diffusion coefficient keeping the QL value. For intermediate values of s_{ov} , where chaos is widespread, the diffusion coefficient D becomes supra-QL for large time: $D \simeq 2.3D_{QL}$ for $s_{ov} \simeq 2.2$ [14]. There is a QL non-chaotic diffusion up to time $t = \tau_{pert}$ and a chaotic non-QL one after τ_{pert} [4, 22, 29]. The existence of this intermediate regime shows that QL estimates for the diffusion coefficient at large s_{ov} do not correspond to a trivial extension of the initial QL regime. Something similar might occur for the regime SNL of the self-consistent case.

As recalled in [appendix A](#), the origin of chaotic diffusion can be understood as the result of locality in the velocity of the wave–particle interaction. The existence of a diffusion over time $\tau_{QL} \gg \tau_{spread}$ enables the rigorous extension of the validity of QL theory up to the time when orbits hit the Kolmogorov–Arnol’d–Moser (KAM) boundaries of the chaotic domain, provided that all the phases φ_m are drawn independently from a uniform distribution on the circle, and the velocity distribution f remains ‘smooth’ (almost constant) over the velocity range Δv_{spec} (no trapping structure) or equivalently the wave spectrum must not be peaked in this velocity (or wavenumber) range [22]: nearby waves may have strongly inhomogeneous amplitudes, but the spectrum should be smooth when averaged over a Dupree width Δv_D (8) (or rather a resonance box width, which is about five times larger, see [appendix A](#)). Indeed mode coupling (e.g. modulational instability) can cause the turbulent wave spectrum to become spikier in k -space (or velocity space) when it grows; and thus it can generate spatial non-uniformity of the velocity distribution function such as small trapping structures (hole versus hump). In order to show that QL theory remains valid in the chaotic regime SNL to describe the nonlinear self-consistent wave–particle interaction, we will show that, when the plateau is formed in the velocity distribution function, mode coupling becomes negligible, and the dynamics lands in the non-self-consistent stage where the wave spectrum meets the assumptions on which QL estimates rest: the independence of phases and a non-peaked amplitude spectrum. To sum up, the final stage of the nonlinear self-consistent waves’–particles’ evolution must satisfy the following three assumptions: a broad enough plateau regime is well settled (negligible mode coupling for waves whose phase velocity belongs to the plateau), the wave spectrum phases are uniformly distributed and independent, the variations of the wave spectrum amplitude are not peaked in velocity.

1.4. Structure of this paper

This paper is organized as follows. Section 2.1 introduces the Vlasov-wave description of the wave–particle interaction. Section 2.2 shows analytically that, if the tail particle distribution displays a plateau, the waves whose phase velocity belongs to the plateau feel a negligible mode coupling in the limit where the plateau is broad enough. Section 2.3 invalidates previous works attempting to prove or to contradict the validity of quasilinear theory in the saturation regime.

Section 3 describes the numerical scheme to approximate the Vlasov-wave models introduced in section 2.1, and determines the simulation parameters. Sections 4 and 5 present self-consistent simulations within the Vlasov-wave description, where the dynamics go from regime L to regime SNL in which QL estimates remain right and accurate.

1.5. Acronyms

- CFL: Courant–Friedrichs–Lewy (condition)
- FP: Fokker–Planck
- INL: intermediate nonlinear (regime)

- L: linear (regime)
- KAM: Kolmogorov–Arnold–Moser
- PT: test particle (simulation)
- QL: quasilinear (regime, theory)
- SNL: strongly nonlinear (regime)

2. Theoretical framework: description of wave–particle self-consistent dynamics

The difficulty in describing the nonlinear regime of the Vlasov–Poisson system of equations and progress in the chaotic dynamics of Hamiltonian systems with a finite number of degrees of freedom were an incentive to tackle the description of the saturation regime with the so-called self-consistent Hamiltonian that describes the one-dimensional self-consistent evolution, in a plasma with spatial periodicity L , of M Langmuir waves with N particles (the beam) in the tail of the electron distribution function per length L [22].

2.1. Self-consistent model

A rigorous classical mechanics calculation [22] allows one to reduce the original N^* -body problem of $N^* \gg 1$ electrostatically coupled particles in a one-dimensional periodic system to a field–particle interaction problem incorporating N resonant particles and M harmonic oscillators defining the field, namely the M Langmuir waves due to the collective vibrations of the bulk (non-resonant particles), assuming $N + M \ll N^*$.

In the absence of tail particles, the Langmuir waves are the collective motions (eigenmodes) of a plasma (without resonant particles) with a density n_p and with a plasma frequency ω_p . Wave m has pulsation ω_m related to the wavenumber k_m through the Bohm–Gross dispersion relation (5). The interaction of these M waves with the N resonant particles is described by the self-consistent Hamiltonian

$$\mathcal{H}_{\text{sc}}^{N,M} = \sum_{n=1}^N \frac{v_n^2}{2} + \sum_{m=1}^M \omega_m \frac{X_m^2 + Y_m^2}{2} + \tilde{\varepsilon} \sum_{n=1}^N \sum_{m=1}^M \frac{\beta_m}{k_m} (Y_m \sin(k_m x_n) - X_m \cos(k_m x_n)) \quad (10)$$

where (x_n, v_n) are the conjugate position and velocity (in fact momentum with mass normalized to unity) of particle n , (X_m, Y_m) are the conjugate generalized coordinate and momentum of the harmonic oscillator corresponding to Langmuir wave m , $\beta_m = [\partial_\omega \mathcal{D}(k_m, \omega_m)]^{-1/2} \simeq 1/\sqrt{2}$, and

$$\tilde{\varepsilon} = \omega_p \sqrt{\frac{2\eta}{(1+\eta)N}}$$

is the coupling coefficient where $\eta = n_b/n_p = N/N^*$. Hamiltonian $\mathcal{H}_{\text{sc}}^{N,M}$ is made up of free particle terms, harmonic oscillator terms and coupling terms. Waves and particles are described on an equal footing: they interact. Hamiltonian (10) is the generalization to $M > 1$ waves [25, 26] of the self-consistent dynamics introduced with $M = 1$ for describing the saturation of the cold beam–plasma instability by Onishchenko *et al* [50] and O’Neil *et al* [49]. It was recast in a Hamiltonian form by Mynick and Kaufman [48] and derived using symplectic formalism by Tennyson *et al* [54]. Finally, Hamiltonian (10) was derived directly for any M from a mechanical description of the plasma as an N -body system [2]. This Hamiltonian (10) generates the evolution equations

$$\dot{x}_n = v_n, \quad (11)$$

$$\dot{v}_n = \tilde{\varepsilon} \operatorname{Re} \left(\sum_{m=1}^M i \beta_m Z_m e^{ik_m x_n} \right), \quad (12)$$

$$\dot{Z}_n = -i \omega_m Z_m + i \tilde{\varepsilon} \frac{\beta_m}{k_m} \sum_{n=1}^N e^{-ik_m x_n}, \quad (13)$$

where the dot denotes time derivative, Re denotes the real part and $Z_m = X_m + iY_m$. Equation (12) makes clear the link between Z_m and the electric field of wave m .

In order to keep some symmetry in the description of waves and particles, but getting rid of granularity effects due to the discrete description of particles (like spontaneous emission of waves by particles which can add difficulty from the numerical point of view [16], non-commutativity of infinite time and infinite number of particles limits [34]), it is easier to work with the so-called Vlasov-wave model which is obtained as a mean-field limit (large- N limit) of the dynamics defined by the Hamiltonian $\mathcal{H}_{\text{sc}}^{N,M}$ [23, 35] in analogy to that performed by Neunzert, Dobrushin, Spohn and others for their elegant and short derivation of the Vlasov equation [53]. If we define the Radon measure (also called the empirical measure) σ_t^N as

$$\sigma_t^N(dx dv) = \frac{L}{N} \sum_{n=1}^N \delta(x - x_n(t)) \otimes \delta(v - v_n(t)) dx dv,$$

and introduce the change of variable

$$\zeta_m = Z_m e^{i\omega_m t} N^{-1/2}, \quad (14)$$

where $(x_n(t), v_n(t), Z_n(t))$ is the solution of the ordinary differential system (11)–(13) then it can be shown [23, 35] that the measure σ_t^N converges weakly (for the topology induced by the dual bounded-Lipschitz distance) as $N \rightarrow \infty$ to an absolutely continuous measure $\mu_t := \sigma_t^\infty$ with density $f(t, x, v)$ provided it converges at $t = 0$, and that the couple $(f, \{\zeta_m\})$ satisfies the following Vlasov-wave (partial differential) equations

$$\partial_t f + v \partial_x f + \varepsilon \operatorname{Re} \left(i \sum_{m=1}^M \beta_m \zeta_m e^{i(k_m x - \omega_m t)} \right) \partial_v f = 0, \quad (15)$$

and

$$\dot{\zeta}_m = i \varepsilon \frac{\beta_m}{k_m} \frac{1}{L} \int_{\Lambda} e^{-i(k_m x - \omega_m t)} f(t, x, v) dv dx, \quad (16)$$

where $\varepsilon = \sqrt{2\eta/(1+\eta)}$, with ω_p normalized to unity and $\Lambda = [0, L] \times \mathbb{R}$.

System (15)–(16) preserves three constants of motion, namely the number of particles, hence the normalization of f (chosen such that $\int f(t, x, v) dv = \mathcal{O}(1)$ for a typical x)

$$\int_{\Lambda} f(t, x, v) dv dx = L, \quad (17)$$

the rescaled total momentum

$$\int_{\Lambda} v f(t, x, v) dv dx + L \sum_{m=1}^M k_m \frac{|\zeta_m|^2}{2} = L \mathfrak{P}, \quad (18)$$

and the rescaled total energy

$$\int_{\Lambda} \left(\frac{v^2}{2} - \varepsilon \operatorname{Re} \left(\sum_{m=1}^M \frac{\beta_m}{k_m} \zeta_m e^{i(k_m x - \omega_m t)} \right) \right) f(t, x, v) dv dx + L \sum_{m=1}^M \omega_m \frac{|\zeta_m|^2}{2} = L \mathfrak{E}. \quad (19)$$

In addition to these ‘mechanical’ constants of the motion, the Vlasov-wave system preserves the usual integral (Casimir) invariants of Vlasov equations like

$$\mathcal{C}_\Theta[f] = L^{-1} \int_\Lambda \Theta(f(t, x, v)) dv dx,$$

for any regular enough function $\Theta : [0, +\infty[\rightarrow \mathbb{R}$. In contrast to (17)–(19), the Casimir invariants do not exist for the singular measures σ^N ; their conservation reflects the fact that, for any wave field (ζ), the dynamics (11)–(12) defines an area-preserving flow in (x, v) space.

In the dense wave spectrum limit, the power spectrum ψ of the waves, as in (2), appears through $\psi(v_m)\Delta v_m = k_m|\zeta_m|^2/2$, where Δv_m is the difference in phase velocity between wave m and its first neighbour. Thus

$$\sum_{\{m \mid u_0 \leq v_m < u_1\}} k_m|\zeta_m|^2/2 \simeq \int_{u_0}^{u_1} \psi(v) dv \quad (20)$$

for any u_0, u_1 . We then define the waves’ total momentum $\mathfrak{P}_w := \sum_{m=1}^M k_m|\zeta_m|^2/2 \simeq \int_{\mathbb{R}} \psi(v) dv$ and waves’ energy $\mathfrak{S}_w := \sum_{m=1}^M \omega_m|\zeta_m|^2/2 \simeq \int_{\mathbb{R}} v\psi(v) dv$.

If the dense spectrum limit is approximated by QL equations (1)–(2), these equations preserve the analogues of (17)–(19), with vanishing coupling energy, and satisfy an H-theorem at the expense of Casimir invariants [22].

2.2. Dynamics when the distribution is a plateau

We now consider [32] the extreme regime SNL where the dynamics defined by (15)–(16) starts at time $t = 0$ with (i) a spectrum of Langmuir waves where all nearby waves are in resonance overlap and (ii) a particle velocity distribution function which is a single broad water bag with a height f_0 over a velocity range including the overlap domain. Both boundaries of the water bag are KAM tori related to the wave field. We first analyse a simplistic description of this dynamics, which will be useful to derive a more accurate one hereafter: (i) the initial condition corresponds to an almost spatially uniform plateau which is kept invariant by the dynamics; (ii) therefore there is no source term for the waves in (16), which keep constant complex amplitudes; (iii) hence the particle dynamics is the one defined by a prescribed spectrum of waves, which preserves the initial plateau. Clumps of particles may experience strong turbulent trapping, but the distribution function is unaffected by this granular effect.

Actually KAM tori, bounding the chaotic domain defined by a prescribed spectrum of waves, experience a sloshing motion due to the waves. This brings a small spatial modulation to the particle density which provides a source term for the Langmuir waves in (16). However, if the plateau is broad, the evolution of the wave spectrum is slow, which brings only a small change to the previous simplistic picture. This slow evolution suggests introducing an adiabatic description of the true dynamic⁴.

To be specific, we consider the case where the waves phase velocities range over an interval $[u_0, u_1]$, the nearest KAM tori have velocities v_a and v_b and the water bag is bounded by KAM tori with velocities $[v_0, v_1]$, with $v_0 \lesssim v_a \lesssim u_0 < u_1 \lesssim v_b \lesssim v_1$ (with typically $s_{\text{ov}} \ll |u_1 - u_0|/\Delta v_\varphi$). Therefore, the plateau width at any position is about $\Delta v_{\text{plat}} = v_1 - v_0$, which is essentially equal to the chaotic domain width $\Delta v_{\text{KAM}} = v_b - v_a$ and to the wave

⁴ These KAM tori are associated with a prescribed spectrum of waves, for which each particle evolves under a 1.5 degrees of freedom Hamiltonian (9). For the self-consistent evolution of waves and particles in the $N + M \gg 1$ degrees of freedom dynamics of (10), phase space is $2(N + M)$ -dimensional and near-integrable behaviour is described by Nekhoroshev’s theorem. The KAM tori no longer bound the motion on large scales, but Arnold diffusion may occur on long-time scales. Note that even the ‘familiar’ Landau damping (in its nonlinear guise) is akin to weak KAM behaviour in the infinite dimensional phase space of the Vlasov–Poisson partial differential equation [46, 47].

spectrum width $\Delta v_{\text{spec}} = u_1 - u_0$. Moreover, assume that the wave numbers are all of comparable order of magnitude, typically k . Particles with velocity v experience the oscillations of a wave m at relative frequencies $\Omega_m = \omega_m - k_m v$, and for a particle or a wave with velocity v the nearest KAM velocity defines $\Omega_{\text{min}} = k \min(v_b - v, v - v_a)$; we denote by $\Delta v_{\text{edge}} = \min(v_1 - u_1, u_0 - v_0)$ the relative velocity of the typical edges of the plateau with respect to the extremal wave velocities. The resonance overlap in the wave spectrum is characterized by the small parameter $1/s_{\text{ov}} \sim \delta\Omega / (k\varepsilon\zeta_*)^{1/2} \ll 1$, where $\delta\Omega \simeq k\Delta v_\varphi$ is the Doppler frequency detuning of two nearby waves and ζ_* is the typical modulus of a wave amplitude.

We now formalize this adiabatic description. Let $\zeta_m(t)$ be the value of ζ_m at time t in the self-consistent dynamics. Consider the non-self-consistent dynamics $D(t_0)$ defined by the self-consistent spectrum of Langmuir waves frozen at time t_0 , as defined by (15) where the ζ_m 's are substituted with the $\zeta_m(t_0)$'s. The chaotic domain $C(t_0)$ in single-particle (Boltzmann or μ) phase space (x, v) defined by this frozen wave spectrum is bounded above and below in v by two KAM tori, respectively, $T_a(t_0)$ and $T_b(t_0)$. The initial particle distribution function $f(x, v, 0)$ is assumed to be uniform on $C(0)$; let f_0 be this uniform value. During the adiabatic evolution corresponding to the true self-consistent dynamics, $f(x, v, t)$ stays uniform on $C(t)$ and keeps the value f_0 . We are left with the calculation of the modulation of the width of a single water bag with height f_0 . The modulation of this width is given by that of KAM tori $T_a(t_0)$ and $T_b(t_0)$, which may be computed by perturbation theory in the typical amplitude ζ_* of the waves.

Since mode–mode coupling is a four-wave process, the first nonvanishing contribution to (16) is of order ζ_*^3 ; we estimate it in appendix B. For waves with phase velocities further than $\mathcal{O}(\Delta v_{\text{edge}})$ from the edges of the plateau, this dominant contribution to $\zeta_m(t)$ scales like a sum of $\varepsilon^4 \beta^4 |\zeta|^3 k / [(v_1 - v_0)\Omega_{\text{min}}^4]$ and $\varepsilon^4 \beta^4 |\zeta|^3 / (8v_1(v_1 - v_0)\Omega_{\text{min}}^2 \delta\Omega)$. Therefore, in the limit of a broad plateau ($\Delta v_{\text{plat}} \rightarrow \infty$) with a fixed discretization $\delta\Omega$, ζ_m will vanish when we consider waves in a central range. If we consider waves near the extremal phase velocity in a moderately wider plateau, the edges must still be Ω_{min}/k away from these waves, which scales at worst like $(\varepsilon\beta\zeta_*)^{2/3}$, which still leaves terms not worse than $\zeta_*^{5/3}/\delta\Omega$ and $\zeta_*^{1/3}$. In the seemingly more dangerous limit $\delta\Omega \rightarrow 0$, the wave evolutions will not depart from adiabaticity before the time scale $\delta\Omega^{-1} \sim \tau_{\text{discr}}$, which tends to infinity. This justifies *a posteriori* our previous adiabatic approximation for all waves.

As a result, the plateau dynamics (further than Ω_{min}/k from its boundaries) is almost the same as in a prescribed field of Langmuir waves. Therefore, the chaotic motion of particles is almost unchanged by the nonlinear coupling of Langmuir waves.

2.3. Inconsistency of several models

We have just shown that self-consistency vanishes in the plateau regime of the bump-on-tail instability if the plateau is broad enough, because the particle transport only rearranges particles without changing f itself within the plateau, depriving waves from this source. This means that the diffusion coefficient $D(v)$ of particles with momentum v is that found for the dynamics of particles in a prescribed spectrum of Langmuir waves. Let $D_{\text{QL}}(v)$ be the QL value of this coefficient. In the resonance overlap regime D/D_{QL} may cover a large range of values [14, 21, 22]. In particular $D \simeq D_{\text{QL}}$ is obtained for random phases of the waves and strong resonance overlap [14, 21, 22, 24]. We stress that strong resonance overlap alone is not enough to provide $D \simeq D_{\text{QL}}$.

Let γ_{L} be the maximum Landau growth rate of Langmuir waves for the instantaneous value of f . As $\tau_{\text{spread}} \simeq 4(k^2 D)^{-1/3}$ is the time after which the ballistic approximation

fails for particles diffusing with the maximum instantaneous D due to a spectrum of waves with typical wavenumber k , the plateau regime corresponds to $\gamma_L \tau_{\text{spread}} = 0$. Since D/D_{QL} may cover a large range of values in this regime, $\gamma_L \tau_{\text{spread}} \ll 1$ does not imply *per se* any renormalization or non-renormalization of D/D_{QL} , nor of γ/γ_L by wave–particle momentum conservation. This contradicts previous works using $\gamma_L \tau_{\text{spread}} \ll 1$ to try and prove the validity of QL theory [22, 29, 43, 44] and the ‘turbulent trapping’ ansatz aiming for the contrary [41]. The value of D/D_{QL} in the plateau regime of the bump-on-tail instability depends on the kind of wave spectrum the beam–plasma system reaches during the regime INL of the instability, and not only on condition $\gamma_L \tau_{\text{spread}} \ll 1$, as assumed by these works. The following numerical simulation using the Vlasov-wave model attempts to uncover this spectrum.

3. Numerical approximation of the Vlasov-wave equation

3.1. Numerical algorithm

Note that the system (15)–(16) admits a unique global regular classical solution, since it is easy to show that the force field is regular for any finite M . Therefore the use of high-order numerical scheme to approximate the system (15)–(16) is relevant.

Here we use a semi-Lagrangian scheme with an (x, v) -area-preserving integrator in time obtained by decomposing the dynamics in integrable Hamiltonian steps. A natural and simple choice is the Strang time-splitting strategy also known as the centred leapfrog symplectic integrator. Roughly speaking, this intensively used scheme (see [7, 9–11, 15, 33] and references therein) consists in splitting the full transport operator into two easily integrable transport operators—one in the physical space, the second one in the velocity or momentum space—and solving them successively in a right order to get high-order approximation in time of the complete transport operator. Moreover B -spline interpolation of high order is used to reconstruct the distribution function on the (x, v) -space mesh and interpolate its values at the origins of the characteristic curves’ set. Such an Eulerian algorithm, usually named Vlasov code, has the advantages of providing an excellent resolution all over the (x, v) space including very low density regions, since convergence and *a priori* high-order accuracy properties of these schemes are well controlled and understood. In addition, conservation of the constants of motion can be ensured with good accuracy by semi-Lagrangian schemes. Although these algorithms cannot capture sub-grid filamentation of the particle distribution function [34], such effects are weak here and appear in slight departures from conservation of mass and other Casimir invariants of f . Moreover, our discussion of dynamics when the distribution is a plateau (section 2.2) stresses that the filamentation issue should not interfere with the wave evolution on which we focus. Recently, mathematical proofs of convergence and *a priori* high-order error estimates (very high-order accuracy) of these schemes were obtained in a series of papers [3, 7, 9, 10].

We discretize the μ -space (x, v) on a grid \mathcal{M}_h with $N_x \times N_v$ mesh points with steps Δx and Δv , and f_h^n an approximation of f at time t^n on \mathcal{M}_h . The general algorithm to compute f_h^{n+1} for $t^{n+1} = t^n + \Delta t$ consists of three steps, consistently coupled to a map evolving the M wave complex amplitudes ζ_m with the same timestep. The algorithm is explicitly described in appendix C.

3.2. Self-consistent simulation parameters

In the next sections we present self-consistent simulations of the Vlasov-wave system (15)–(16). In order to construct relevant test cases to assess the validity of QL theory, we

must estimate some physical parameters. Moreover, since the plateau formation in the strong chaotic regime could take a very long time, we need to optimize the values of physical and numerical parameters; hence *a priori* estimates for these parameters are required. They are based on momentum conservation since we can clearly separate the two contributions of the waves and particles. In contrast, the use of energy conservation is not appropriate because it involves a third term, associated with the wave–particle coupling, which is more difficult to estimate *a priori*.

Since $k_m \lambda_D \ll 1$, using the Bohm–Gross relation we deduce that $\omega_m \simeq \omega_p = 1$. Therefore, the phase velocity range of interest will be $v_\varphi \in [u_0, u_1] = [k_{\max}^{-1}, k_{\min}^{-1}]$, with a width $\Delta v_{\text{spec}} = u_1 - u_0$. From the (x, v) -area conservation and the normalization of the distribution function, the height of the particle velocity distribution function plateau in the long-time asymptotic regime is approximately $(u_1 - u_0)^{-1}$ (to first approximation, neglecting the particles which might be outside the wave velocity range as they are weakly perturbed by the waves). We assume

$$k_m = \frac{2\pi}{L}(v_0 + m), \quad \text{with } m \in [1, M],$$

so that $v_{\varphi,m} = \omega_p/k_m = 1/k_m$ which implies

$$u_0 = \frac{v_0 + 1}{M - 1} \Delta v_{\text{spec}} \simeq \frac{v_0}{M} \Delta v_{\text{spec}},$$

$$u_1 = \frac{L}{2\pi(v_0 + 1)} \simeq \left(1 + \frac{v_0}{M}\right) \Delta v_{\text{spec}},$$

$$L = 2\pi(v_0 + M)u_0 \simeq 2\pi \left(1 + \frac{v_0}{M}\right) v_0 \Delta v_{\text{spec}},$$

$$\frac{2\pi M}{L} = \left(1 + \frac{v_0}{M}\right)^{-1} u_0^{-1} \simeq \left(\left(1 + \frac{v_0}{M}\right) \frac{v_0}{M} \Delta v_{\text{spec}}\right)^{-1},$$

where we assumed $v_0 \gg 1$ and $M \gg 1$. Using momentum conservation (18), assuming that the initial (respectively final) distribution function f_0 (respectively f_∞) is homogeneous in space, and neglecting $\psi(0, v)$ we obtain

$$\begin{aligned} \mathfrak{P}_w^\infty - \mathfrak{P}_w^0 &= \int_{u_0}^{u_1} v(f_0 - f_\infty) dv = \int_{u_0}^{u_1} \psi(\infty, v) dv \\ &= \sum_{m=1}^M \psi(\infty, v_m) \Delta v_m = \sum_{m=1}^M k_m \frac{|\zeta_m(\infty)|^2}{2} \\ &= \int_{k_{\min}}^{k_{\max}} \Psi(\infty, k) dk = \sum_{m=1}^M \Psi(\infty, k_m) \Delta k_m \end{aligned} \quad (21)$$

where we used (20) and $\Psi(t, k) = \psi(t, v)|dv/dk|$ to express the power spectrum of waves with respect to wavenumber. Equation (21) can also be obtained by integrating the conservation law

$$\partial_t v(t, v) = 0 \quad (22)$$

with

$$v(t, v) = f(t, v) - \partial_v \psi(t, v)$$

(which follows [22] from QL equations (1)–(4)) with the initial condition $\partial_v \psi(0, v) = 0$ and the boundary condition $\psi(t, u_0) = \psi(t, u_1) = 0$.

3.3. Estimates of physical parameters

We first estimate a mean value (denoted by $\langle a \rangle = M^{-1} \sum_m a_m$ for any variable a) of the wave power spectrum at the final time where the plateau regime is well settled. Since $\Delta k_m = k_{m+1} - k_m = 2\pi/L$, we have $\mathfrak{P}_w^\infty - \mathfrak{P}_w^0 \simeq (1 + \frac{v_0}{M})^{-1} v_0^{-1} \Delta v_{\text{spec}}^{-1} \sum_{m=1}^M \Psi(\infty, k_m)$ and thus

$$\langle \Psi(\infty) \rangle \simeq \left(1 + \frac{v_0}{M}\right) \frac{v_0}{M} \Delta v_{\text{spec}} (\mathfrak{P}_w^\infty - \mathfrak{P}_w^0). \quad (23)$$

Since $D_{\text{QL}}(t, v_m) \simeq \pi \eta \beta_m^2 |\zeta_m|^2 (k_m \Delta v_m)^{-1} = 2\pi \eta \beta_m^2 k_m^{-2} \psi(t, v_m) \simeq \pi \eta \Psi(t, k_m)$, using (23) we obtain for the QL diffusion coefficient

$$\langle D_{\text{QL}}(\infty) \rangle \simeq \pi \eta \left(1 + \frac{v_0}{M}\right) \frac{v_0}{M} \Delta v_{\text{spec}} (\mathfrak{P}_w^\infty - \mathfrak{P}_w^0) \quad (24)$$

which determines the characteristic time τ_D (6).

Then we estimate the Kubo-like number. As $K_{D,m}^{-1}$ estimates the number of velocity diffusion widths through the wave spectrum at saturation, we shall test the condition $K_{D,m}^{-1} \gg 1$. Using (24) we obtain

$$K_{D,m}^{-1} \simeq \langle K_{D,m}^{-1} \rangle = \Delta v_{\text{spec}} \langle (k_m / D_{\text{QL},m})^{1/3} \rangle \simeq \Delta v_{\text{spec}} \langle k_m^{1/3} \rangle \langle D_{\text{QL},m} \rangle^{-1/3},$$

where, for $\alpha \neq -1$,

$$\begin{aligned} \langle k_m^\alpha \rangle &\simeq \frac{L}{2\pi M} \int_{k_{\min}}^{k_{\max}} k^\alpha dk = \frac{L}{2\pi M} \frac{k_{\max}^{\alpha+1} - k_{\min}^{\alpha+1}}{\alpha+1} \\ &\simeq \frac{L}{2(1+\alpha)\pi M \Delta v_{\text{spec}}} \left(\left(\frac{v_0}{M}\right)^{-(\alpha+1)} - \left(1 + \frac{v_0}{M}\right)^{-(\alpha+1)} \right). \end{aligned}$$

We also estimate the parameter \mathcal{B}^{-1} . From $\Delta v_{\varphi,m} \simeq 2\pi/(Lk_m^2)$ (as k_m varies linearly with m) we obtain $\mathcal{B}_m^{-1} = \Delta v_{D,m}/(\Delta v_{\varphi,m}) = D_{\text{QL},m}^{1/3} k_m^{5/3} L/(2\pi)$ and

$$\mathcal{B}^{-1} \simeq \langle \mathcal{B}_m^{-1} \rangle = \frac{L}{2\pi} \langle k_m^{5/3} D_{\text{QL},m}^{1/3} \rangle \simeq \frac{L}{2\pi} \langle D_{\text{QL},m} \rangle^{1/3} \langle k_m^{5/3} \rangle.$$

The parameter \mathcal{B}_m (relevant to the strong overlap regime of many waves) is related to the more familiar Chirikov resonance overlap parameter $s_{\text{ov},m} = (512/\pi)^{1/4} \mathcal{B}_m^{-3/4} \simeq 3.6 \mathcal{B}_m^{-3/4}$ (more appropriate for few waves overlapping moderately). Again,

$$s_{\text{ov}} = \langle s_{\text{ov},m} \rangle \simeq 8\sqrt{\pi} L^{-3/4} \langle D_{\text{QL},m} \rangle^{-1/4} \langle k_m^{-5/4} \rangle.$$

Finally note that $\mu \ll 1$ at the beginning of the instability and $\mu \gg 1$ in the saturation phase. To ensure that $\mu \ll 1$ at the beginning, it is equivalent to guarantee that we have an initial linear regime where wave m grows exponentially with the Landau growth rate

$$\gamma_{L,m} = \gamma_L(0, v_m) = \frac{\pi}{2} \frac{\eta}{1+\eta} v_m^2 \partial_v f_0(v_m).$$

In order to ensure that $\mu \gg 1$ at the end of the simulation we verify that the plateau regime settled in, with a final distribution function f almost constant in velocity. Although these estimates are crude ($\langle ab \rangle \sim \langle a \rangle \langle b \rangle$), they capture the relevant scaling powers for the subsequent discussion.

3.4. Estimates of numerical parameters

We now estimate the numerical parameters of the simulations. Our mesh \mathcal{M}_h is a regular Cartesian grid spanning $[0, L] \times [v_{\min}, v_{\max}]$. Boundary conditions are periodic in space x , while the range $[v_{\min}, v_{\max}]$ must contain both the whole spectrum of wave phase velocities

$[u_0, u_1]$ and the support of the particle distribution function during the whole simulation. Thus $v_{\min} < u_0 < u_1 < v_{\max}$ in such a way that $f(t, x, v_{\min}) = f(t, x, v_{\max}) = 0$ for all (t, x) . In terms of section 2.2 we thus need $v_{\min} < v_0 < v_1 < v_{\max}$. We might estimate $v_{\min} \leq u_0 - n_{\text{KAM}} s_{\text{ov}} \Delta v_\varphi$ and $v_{\max} \geq u_1 + n_{\text{KAM}} s_{\text{ov}} \Delta v_\varphi$ for some real positive $n_{\text{KAM}} > 2$.

Let us define Δx (respectively Δv) as the space discretization step (respectively the velocity discretization step) for the mesh \mathcal{M}_h . We set Δx as the ratio of the shortest length $2\pi/k_{\max}$ we need to resolve to $n_{\delta x}$ with $n_{\delta x} \geq 1$ a positive real number. Similarly we set Δv as the ratio of a typical phase velocity difference $\Delta v_\varphi = \langle \Delta v_{\varphi, m} \rangle \simeq \Delta v_{\text{spec}}/M$ to $n_{\Delta v_\varphi}$ with $n_{\Delta v_\varphi} \geq 1$ a positive real number. So we obtain

$$\Delta x = \frac{2\pi}{n_{\delta x} k_{\max}} \simeq \frac{2\pi}{n_{\delta x}} \frac{v_0}{M} \Delta v_{\text{spec}}, \quad N_x = \frac{L}{\Delta x} \simeq n_{\delta x} (v_0 + M)$$

and

$$\Delta v = \frac{\Delta v_\varphi}{n_{\Delta v_\varphi}} \simeq \frac{\Delta v_{\text{spec}}}{M n_{\Delta v_\varphi}}, \quad N_v = \frac{\Delta v_{\text{spec}}}{\Delta v} \simeq n_{\Delta v_\varphi} M.$$

Next we estimate the time step Δt . There are two ways for estimating this parameter and we will see that they give equivalent results. From purely numerical considerations we can estimate Δt by setting the Courant–Friedrichs–Lewy (CFL)-like condition $\Delta x \sim v_{\max} \Delta t$. By taking $v_{\max} = u_1$ we obtain

$$\Delta t = u_1^{-1} \Delta x \simeq \frac{2\pi}{n_{\delta x}} \frac{v_0}{M} \left(1 + \frac{v_0}{M}\right)^{-1}. \quad (25)$$

We must stress that semi-Lagrangian schemes are unconditionally stable and therefore no CFL condition is required to ensure the stability of the scheme. Nevertheless, in order to guarantee accurate numerical results, in practice we have to ensure that the numerical and physical velocities of waves are of the same order, which leads to the CFL-like condition (25).

From physical considerations the time step Δt must be chosen such that phase $\Phi_m = k_m x - \omega_m t$ of wave m does not vary too much over time Δt . In practice this condition is required so that the discretized force field which appears in the Vlasov-wave equations (15)–(16) is sufficiently well sampled. Therefore, we must have $\max \Delta \Phi_m = 2\pi/n_\phi$ with $n_\phi \geq 1$ a positive real number, with

$$\begin{aligned} \max |\Delta \Phi_m| &= \Delta t \max \left| k_m \frac{\Delta x}{\Delta t} - \omega_m \right| = \Delta t \max |k_m v - \omega_m| \\ &= \Delta t |k_{\max} v_{\max} - 1| \simeq \Delta t |k_{\max} u_1 - 1| \simeq \Delta t \left(\frac{v_0}{M} \right)^{-1}. \end{aligned}$$

As a consequence we get

$$\Delta t \simeq \frac{2\pi}{n_\phi} \frac{v_0}{M}. \quad (26)$$

The time step estimates (25) and (26) are equivalent provided that $v_0/M \ll 1$, which will be the case. Finally we can estimate the final time T_{end} as

$$T_{\text{end}} \propto \max\{(\gamma_{\text{L}}(0))^{-1}, T_{\text{dif}}\},$$

where

$$T_{\text{dif}} = \frac{\langle \Delta v_{\text{spec}}^2 \rangle}{2 \langle D_{\text{QL}}(\infty) \rangle} \simeq \Delta v_{\text{spec}} \left(2\pi \eta \left(1 + \frac{v_0}{M}\right) \frac{v_0}{M} (\mathfrak{P}_w^\infty - \mathfrak{P}_w^0) \right)^{-1},$$

while we take

$$\langle \gamma_{\text{L}}(0) \rangle = \frac{\pi}{2} \frac{\eta}{1 + \eta} (u_1 - u_0)^{-1} \int_{u_0}^{u_1} v^2 \partial_v f_0(v) \, dv \simeq \frac{\pi}{3} \frac{\eta}{1 + \eta} \frac{u_1^3 - u_0^3}{(u_1 - u_0)^3},$$

for an initial triangular distribution function, and $\langle \gamma_L(0) \rangle$ as a prescribed constant for an initial hyperbolic distribution function (see the next sections). The number of time iterations is set to $N_T = T_{\text{end}}/\Delta t$.

3.5. Asymptotic estimates for all the parameters

Finally we find the asymptotic expression for the parameters defined in sections 3.3 and 3.4 when we consider $v_0/M \ll 1$ and $u_1 = 1$ which implies $\Delta v_{\text{spec}} = (1 + (v_0/M))^{-1} \simeq 1$. We obtain (up to factors close to unity, such as $\pi^{1/3}$)

$$\begin{aligned} \langle \Psi(\infty) \rangle &\simeq \left(\frac{v_0}{M}\right) (\mathfrak{P}_w^\infty - \mathfrak{P}_w^0), \\ \langle D_{\text{QL}}(\infty) \rangle &\simeq \pi \eta \langle \Psi(\infty) \rangle \simeq \pi \eta \left(\frac{v_0}{M}\right) (\mathfrak{P}_w^\infty - \mathfrak{P}_w^0), \\ K_{\text{D}}^{-1} &\simeq 1/\Delta v_{\text{D}} \simeq \eta^{-1/3} \left(\frac{v_0}{M}\right)^{-2/3} (\mathfrak{P}_w^\infty - \mathfrak{P}_w^0)^{-1/3}, \\ \mathcal{B}^{-1} &\simeq \eta^{1/3} \left(\frac{v_0}{M}\right)^{-4/3} v_0 (\mathfrak{P}_w^\infty - \mathfrak{P}_w^0)^{1/3}, \\ N_x &\simeq \left(\frac{v_0}{M}\right)^{-1} v_0 n_{\delta x} = M n_{\delta x}, \\ N_v &\simeq \left(\frac{v_0}{M}\right)^{-1} v_0 n_{\Delta v_\varphi} = M n_{\Delta v_\varphi}, \\ \Delta t &\simeq \frac{2\pi}{n_\Phi} \left(\frac{v_0}{M}\right), \\ T_{\text{end}} &\simeq \max \{ \langle \gamma_L(0) \rangle^{-1}, T_{\text{dif}} \} \simeq \max \{ \eta^{-1}, \langle D_{\text{QL}}(\infty) \rangle^{-1} \}. \end{aligned}$$

We first note that, given the wavenumbers k_m and the dispersion relation, the ratio $\tau_{\text{discr}}/\tau_{\text{ac}} = \Delta v_{\text{spec}}/\Delta v_\varphi = M$ is independent of the waves and particles' evolutions, and we need a large ratio to allow observations of intermediate scales like τ_{D} or Δv_{D} . Constraint $\eta \ll 1$ is also desired to ensure that $\mu \ll 1$ initially, and that both γ_L/ω_p and D_{QL} be small when $\partial_v f$ and ψ are of the order of unity.

From these asymptotic values we observe that conditions $\eta \ll 1$ and $v_0/M \ll 1$ work towards ensuring a small value for the Kubo number K_{D} and the Dupree width Δv_{D} (which means several resonance boxes in the wave velocity range, see [appendix A](#)). On the other hand, conditions $\eta \gg 1$, $v_0 \gg 1$ and $v_0/M \ll 1$ favour a strong resonance overlap parameter so that $\mathcal{B}^{-1} \gg 1$.

Therefore we choose η , v_0 and M , under the constraints $\eta \ll 1$ and $v_0/M \ll 1$, such that K_{D} and Δv_{D} are sufficiently small while $v_0/M \lesssim \eta^{1/4}$ is small enough and $v_0 \gg 1$ is large enough to balance the small value of η in the estimate for \mathcal{B} and so ensure a small value for this latter parameter.

4. Hyperbolic case

Following Doxas and Cary [16] we choose an initial distribution function f_0 such that the Landau growth rate is uniform in velocity. This choice is interesting for several reasons. It enables (i) a simple validation of the numerical description of the linear regime; (ii) all waves (with various phase velocities) to enter more or less together into the nonlinear regime by choosing initial amplitudes provided by the saturation amplitude predicted by QL theory,

downscaled by a (small) factor ϵ_{ζ^0} independent of the velocity; (iii) continuity with the work [16]. Since

$$\gamma_{\text{L}}(0, v) = \frac{\pi}{2} \frac{\eta}{1 + \eta} v^2 \partial_v f_0(v),$$

we obtain for all $v \in [u_0, u_1]$,

$$f_0(v) = C_1 + C_2 \left(1 - \frac{u_0}{v}\right),$$

where

$$C_2 = \frac{2\gamma_{\text{L}}(1 + \eta)}{\eta\pi u_0} \quad \text{and} \quad C_1 = \frac{1 + C_2 \left[u_0 \ln \left(\frac{u_1}{u_0} \right) - u_1 + u_0 \right]}{u_1 - u_0}.$$

From momentum conservation we get

$$\mathfrak{P}_{\text{w}}^{\infty} - \mathfrak{P}_{\text{w}}^0 = (u_1 - u_0) \left(\frac{u_0 + u_1}{2} (C_1 + C_2) - C_2 u_0 \right) - \frac{u_0 + u_1}{2}.$$

We initialize the wave amplitudes by setting

$$|\zeta_m| = \epsilon_{\zeta^0} \sqrt{2\psi_{\infty}(v_m) \frac{\Delta v_m}{k_m}}, \quad (27)$$

where, for all $v \in [u_0, u_1]$,

$$\psi_{\infty}(v) = \int_{u_0}^v (f_{\infty}(\xi) - f_0(\xi)) d\xi = \left(\frac{1}{u_1 - u_0} - C_1 - C_2 \right) (v - u_0) + C_2 u_0 \ln \left(\frac{v}{u_0} \right), \quad (28)$$

with ϵ_{ζ^0} a sufficiently small positive real number such that an initial linear regime with an exponential growth of waves could exist. Equation (28) is obtained by integrating conservation law (22) with initial condition $\partial_v \psi(0, v) = 0$ and boundary condition $\psi(t, u_0) = 0$.

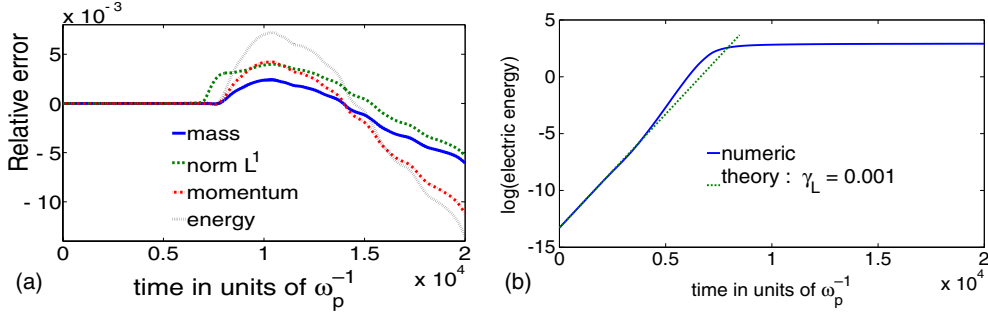
Therefore, we choose an initial wave spectrum $\{\zeta_m\} = \{(\text{Re } \zeta_m, \text{Im } \zeta_m)\} = \{(|\zeta_m| \cos \varphi_m, |\zeta_m| \sin \varphi_m)\}$, such that wave amplitudes $|\zeta_m|$ are given by (27) and phases φ_m are given by independent uniformly distributed real-valued random variables on the circle (i.e. with $1/(2\pi)$ for probability density). The physical parameters of the simulations are $\omega_p = 1$, $\nu_0 = 75$, $M = 450$, $\gamma_{\text{L}}(0) = 10^{-3}$, $\eta = 2.55 \times 10^{-3}$, $T_{\text{end}} = 10^4$ ($\simeq 2 \max\{(\gamma_{\text{L}}(0))^{-1}, T_{\text{dif}}\}$), $L_x = 152\pi$, $v_{\text{min}} = 0$ and $v_{\text{max}} = 8/7$. The numerical parameters of the simulations are $N_x = 2112$ ($n_{\delta x} \simeq 4$), $N_v = 768$ ($n_{\Delta v_{\varphi}} \simeq 1$), $\Delta t = 0.25$ ($n_{\phi} \simeq 4$) and $\epsilon_{\zeta^0} = \exp(-8)$. Using the coarse estimates of section 3.4 we get the *a priori* estimates for the plateau regime $K_{\text{D}}^{-1} \simeq 30$, $s_{\text{ov}} \simeq 50$ (or $\mathcal{B}^{-1} \simeq 36$) and $\Delta v_{\text{D}} \simeq 3. \times 10^{-2}$. Finally we have $u_0 = 0.145$, $u_1 = 1$, $k_{\text{min}} = 1$, $k_{\text{max}} \simeq 6.91$ and $\Delta v_{\text{spec}}^{-1} \simeq 1.17$.

In contrast to [16] we do not impose a dense wave spectrum, with $s_{\text{ov}} \gg 1$, at initial time: $s_{\text{ov},m}(0) \simeq s_{\text{ov}}(T_{\text{end}}) \sqrt{\epsilon_{\zeta^0}} \simeq 50 \exp(-4) \simeq 1$. Moreover, our initial wave amplitudes are not tuned to imply a v -independent D_{QL} , but rather to fit the wave power spectrum in the plateau regime, as predicted by QL equations. The reason for this difference is that we do not focus specifically on regime INL to monitor γ/γ_{L} but rather on regime SNL reached in the plateau, where we want to compute D/D_{QL} for $\mu \rightarrow \infty$. However, we use the INL behaviour to benchmark our simulation with respect to [16].

Table 1 sums up the parameter values used here (denoted B.E.E.B.) and in [16] (denoted D.C.) for the hyperbolic test case. The first three lines recall fixed parameters. The subsequent lines compare physical quantities γ , μ , s_{ov} , K_{D} at specific times in regime INL, at which the current wave growth rate γ differs most from the Landau growth rate (two points S_1 and S_2 are considered for B.E.E.B. depending on the definition of average rates).

Table 1. Comparison of physical parameters at time where γ/γ_L is maximum between our test case (B.E.E.B.) and test case of [16] (D.C.).

Test case	B.E.E.B. S_1	B.E.E.B. S_2	D.C.
M	450	450	584
γ_0	10^{-3}	10^{-3}	6.25×10^{-5}
η	2.55×10^{-3}	2.55×10^{-3}	4.1×10^{-6}
$\max \gamma/\gamma_{L,1}$	1.29	1.36	1.32
μ	22	56	39
s_{ov}	12	20	14
K_D^{-1}	1950	660	94


Figure 1. (a) Relative error in conservation laws. (b) Continuous blue line: logarithm of waves' total energy \mathcal{H}_w ; dotted green line: extrapolation at initial linear rate. (Colour online.)

4.1. Validation of the linear and nonlinear regimes

This subsection is devoted to the code validation in the linear and nonlinear regimes. All figures refer to a single, typical realization of the dynamics.

We observe in figure 1(a) that mass is conserved with a relative error less than 0.25% up to time $1.6 \times 10^4 \omega_p^{-1}$. The conservation of the L^1 -norm, which measures the importance of negative values in the distribution function, is very good since up to time $1.9 \times 10^4 \omega_p^{-1}$ it is preserved with a relative error less than 0.4%. The conservation laws of momentum and energy are well respected, since momentum is conserved with a relative error less than 0.42% up to time $1.58 \times 10^4 \omega_p^{-1}$, while energy is conserved with a relative error less than 0.7% up to time $1.73 \times 10^4 \omega_p^{-1}$. Figure 2 shows the shares of the total momentum and energy between wave, particle and coupling terms. Wave-particle coupling energy remains negligible, which supports the strong randomness picture of the microscopic dynamics in the nonlinear regimes. Over the whole evolution, momentum transfer from particles to waves is about 1/6 of the total momentum.

Next we benchmark our simulation by checking the initial regime L. Since every wave grows exponentially in the linear stage with the same growth rate by construction, we can compare directly this theoretical growth rate with the growth rate of the waves' total energy \mathcal{H}_w . Figure 1(b) shows that the theoretical growth rate of the waves coincides perfectly with the numerical one until time $t = 2000 \omega_p^{-1}$, which means that the system actually starts with an initial linear stage characterized by $\mu \ll 1$ with a duration of $2000 \omega_p^{-1} = 2/\gamma_L(0)$. This observation of the waves' total energy, and of its growth rate $\gamma(t) := (2\mathcal{H}_w)^{-1} \frac{d}{dt} \mathcal{H}_w$, will be confirmed below, by the analysis of the growth of all waves individually in figure 4.

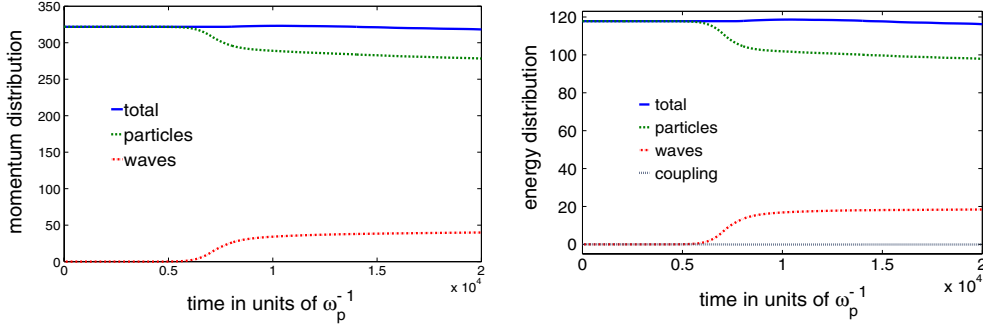


Figure 2. Sharing of momentum and energy between particles (green), waves (red) and coupling (light blue). (Colour online.)

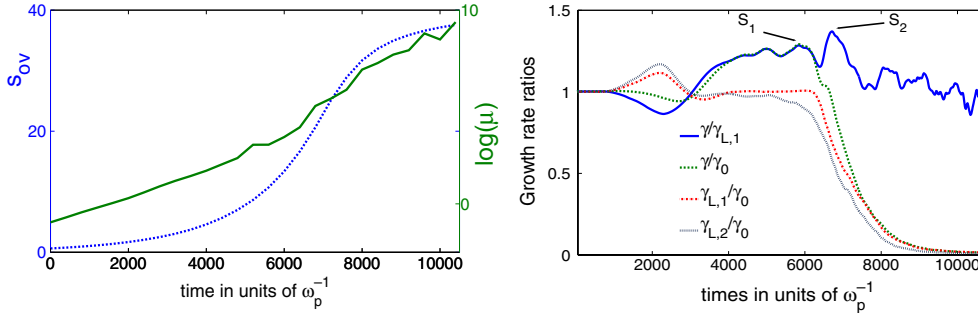


Figure 3. (Left) time evolution of nonlinearity parameters μ (continuous green line) and s_{ov} (dotted blue line). (Right) evolution of γ/γ_L , $\gamma/\gamma_L(0)$ and $\gamma_L/\gamma_L(0)$. Here the energy growth rate is $\gamma(t) = (2E_w(t))^{-1} dE_w(t)/dt$, where $E_w(t) = \sum_{m=10}^M |\zeta(t, v_m)|^2$ (with $v_{10} \simeq 0.9$). Two average Landau growth rates are plotted, namely $\gamma_{L,1}(t) = (\sum_{m=10}^M \Delta v_m)^{-1} \sum_{m=10}^M \gamma_L(t, v_m) \Delta v_m$ and $\gamma_{L,2}(t) = (\sum_{m=10}^M |\zeta(t, v_m)|^2)^{-1} \sum_{m=10}^M \gamma_L(t, v_m) |\zeta(t, v_m)|^2$. The initial value is $\gamma_L(0) = 10^{-3}$. (Colour online.)

From time $t = 2000\omega_p^{-1}$ to $t = 7000\omega_p^{-1}$ we observe an intermediate regime where the wave growth rates depart from Landau's linear approximation (see figures 1(b), 3 and 4): as noted by [16], mode coupling is present, and this intermediate stage corresponds to the transition regime INL, where parameter μ increases from a small value to a value of the order of unity or larger, and s_{ov} increases from a moderate value to a large one. Because the particle velocity distribution function does not flatten at the same rate at all velocities, the Landau growth rate depends on v , and we monitor two average rates, namely a crude average $\gamma_{L,1}(t) = (\sum_{m=10}^M \Delta v_m)^{-1} \sum_{m=10}^M \gamma_L(t, v_m) \Delta v_m$ and an intensity-based average $\gamma_{L,2}(t) = (\sum_{m=10}^M |\zeta(t, v_m)|^2)^{-1} \sum_{m=10}^M \gamma_L(t, v_m) |\zeta(t, v_m)|^2$, discarding the contribution of waves too close to the 'plateau' edge (which we saw in section 2.2 to possibly behave differently from the bulk of the wave spectrum, and which are affected here by the steepening of f , see figure 5). Both average rates behave similarly, and we shall not dwell on their differences as our simulations were tailored to assess a possible renormalization of the diffusion coefficient in the plateau regime. During the beginning of this regime, the perturbative calculation of [39] makes likely the occurrence of an enhanced growth rate. What is striking is the growth rate enhancement⁵ by a factor greater than 1.2 over the interval $t \in [4000\omega_p^{-1}, 7000\omega_p^{-1}]$, with a

⁵ The small decrease of γ for $2000 < \omega_p t < 3000$ (with $\gamma/\gamma_0 \sim 0.95$, $\mu \simeq 2.1$ and $s_{ov} \simeq 2.2$) remains tolerable in our benchmarking, as [16] also obtains $\gamma/\gamma_0 \sim 0.98$ with $\mu \simeq 2.2$ and $s_{ov} \simeq 14$.

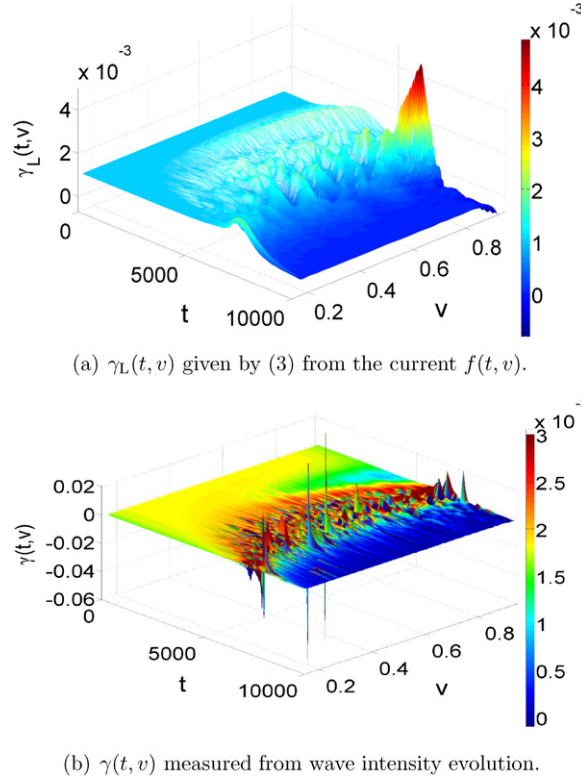


Figure 4. Time evolution of the waves' growth rates. (Colour online.)

maximum factor 1.36 at time $t = 6731\omega_p^{-1}$ ($\mu \simeq 56$, $s_{ov} \simeq 20$), confirming the saturation value emerging in [16] (see table 1). This enhancement contradicts the analytical argument for the validity of QL theory in [52], since our numerical calculation involves the averages over a Dupree width. Actually, assessing [52] does not even require such an average, as the wave intensities are a smooth function of velocity for this run in this time range. This enhanced growth rate by 1.36 may be related to the enhanced particle transport (by up to $2.3 \simeq 1.36^3$, see the scaling $\tau_D \sim D^{-1/3}$) in a given wave field (9) with smooth intensity and random phases [14, 21].

We next observe a nonlinear saturation stage from time $t = 7000\omega_p^{-1}$ to $t = 20000\omega_p^{-1}$, where the plateau is set up by $t = 8400\omega_p^{-1}$, in figures 1(b), 4 and 5.

In figure 3, we observe that for relatively large values of μ , typically $\mu \simeq 56$, the ratio γ/γ_L is around 1.36 (see table 1). In [43, 44] the authors obtain an analytical formula (equation (38) in [44]) for such a renormalization factor γ_{ren} which scales like $\gamma_{ren} = 1 + A\gamma_L/\omega_p$ in the regime where $\mu \gg 1$, with a factor A of the order of unity. Of course this asymptotic expression of γ_{ren} holds in the plateau regime since in this case $\gamma_L \simeq 0$. Nevertheless, equation (38) in [44] is not compatible with the result of figure 3 since, in the regime where $\mu \gg 1$, there exists an intermediate stage (regime INL) where we observe an enhancement of the growth rate with a factor around 1.36. This enhancement is significantly smaller than the turbulent trapping estimate which may be as large as 2. Yet a more detailed inspection in figure 4 of the growth rate $\gamma(t, v) = \frac{1}{2}\psi^{-1}d\psi/dt = |\zeta|^{-1}d|\zeta|/dt$ shows that the ratio 1.2...1.36 merely reflects

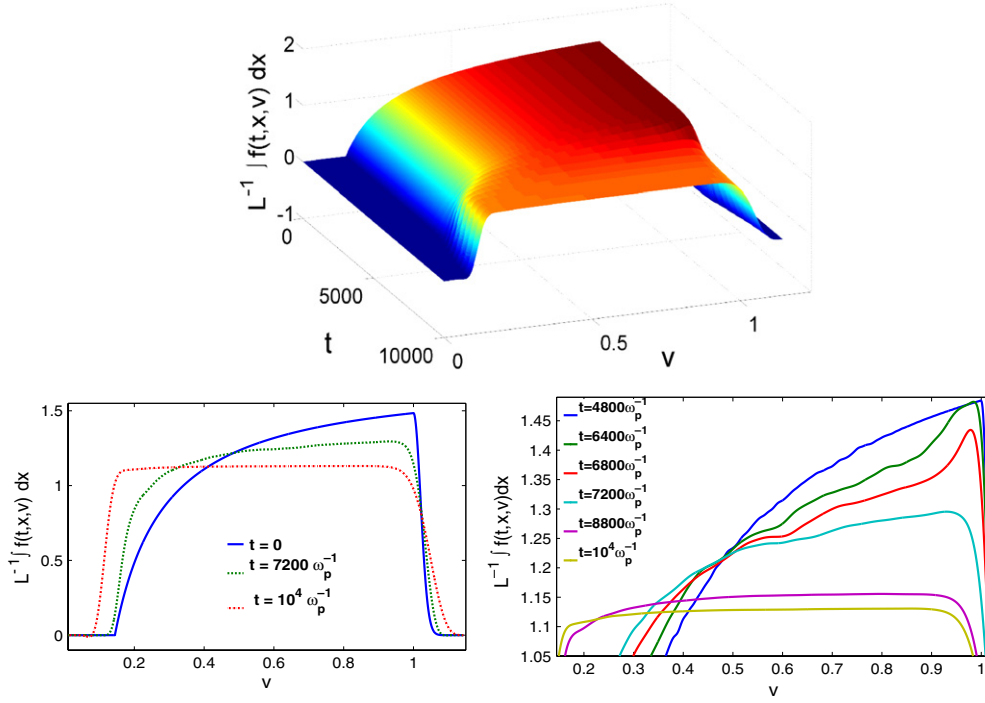


Figure 5. Plateau formation in the x -averaged velocity distribution function. (Colour online.)

average behaviour, and that actually the wave intensities burst quite violently but also quite independently of each other during this time range.

Finally, figure 3 (right) shows that after a period where the enhancement factor increases to its maximum value 1.36, there exists a second stage where this factor decreases, which means that the enhancement process breaks down after a certain time in the INL regime. This result contradicts the hypothesis of [44], according to which the enhanced growth rate or the enhanced diffusivity could be the result of an artificial effect caused by imposing periodic boundary conditions in numerical simulations. Therefore, periodicity does not seem here to impact artificially the enhancement of nonlinear effects (furthermore, if it had such an impact, the argument would also apply in the plateau regime—which it clearly does not, see below).

Note that when the plateau is settled, say for times $t > 8000\omega_p^{-1}$, both γ and γ_L are small, so that their ratio becomes numerically less meaningful.

4.2. Transition from stochastic to chaotic diffusion

After discussing the global aspects of the Vlasov-wave system evolution, we turn to more detailed behaviour, resolved in velocity v .

From figure 5 we observe that the space-averaged distribution function evolves from the hyperbolic shape to the plateau one between times $t \simeq 4800\omega_p^{-1}$ and $t \simeq 8400\omega_p^{-1}$; the plateau appears near the centre of the velocity distribution and erodes the higher values of f causing the increase in the wave growth rate for faster phase velocities. Simultaneously the growth rate of every wave falls from a strictly positive value to a vanishing one (see figure 4). This means that the plateau regime is reached by time $t \simeq 8400\omega_p^{-1}$, as confirmed by figure 6.

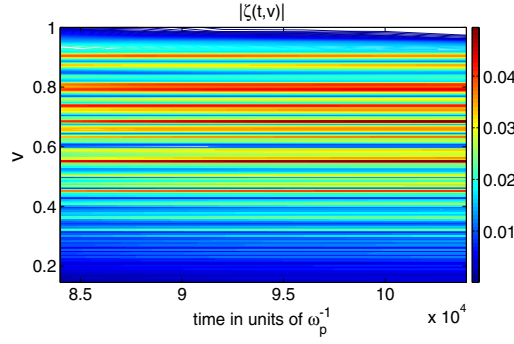


Figure 6. Wave amplitudes for a single realization in the plateau regime, between times $t = 8400\omega_p^{-1}$ and $t = 10400\omega_p^{-1}$. (Colour online.)

In figure 7 we analyse the velocity profiles of QL diffusion coefficient. The smooth curves are the theoretical predictions (4) obtained by integrating the conservation law (22) with initial condition $\partial_v \psi(0, v) = 0$ and boundary condition $\psi(t, u_0) = 0$. We compare this prediction with the result of a single realization of initial data (figure 7, top), and with the average spectrum for a statistical ensemble comprising $R = 210$ realizations of the same Vlasov-wave test case where random initial phases are drawn independently from a uniform distribution on the circle (figure 7, bottom). In the following the bracket notation $\langle \cdot \rangle_R$ means that averaging over a statistical ensemble of R realizations has been performed. In figure 7 (right) the ‘avg’ subscript means that we carried out a floating average of five wave half-widths, namely we set (with $L_{\text{avg}} = 5$)

$$D_{\text{QL, avg}}(v_m) = \sum_{\ell=-L_{\text{avg}}}^{L_{\text{avg}}} \frac{D_{\text{QL}}(v_m) \Delta v_{\varphi, m+\ell}}{v_{\varphi, m+L_{\text{avg}}+1} - v_{\varphi, m-L_{\text{avg}}}}. \quad (29)$$

From figure 7 in the plateau regime, we observe quite good agreement between the QL prediction of the diffusion coefficient (and hence the wave spectrum) and the one obtained by self-consistent simulations of the Vlasov-wave model.

In order to verify that we are in regime SNL where chaotic diffusion applies, we need to look at the value of the Kubo parameter K_D , of the Chirikov resonance overlap parameter s_{ov} (or \mathcal{B}^{-1}) and of parameter μ . From figure 8 we notice that at the middle of the phase velocity range of the wave spectrum, i.e. for $v_c = (u_0 + u_1)/2 \simeq 0.57$ and at time $T = 10^4 \omega_p^{-1}$ in the plateau regime, we have $\langle s_{\text{ov}} \rangle_R(T, v_c) \simeq 22$, $\langle K_D^{-1} \rangle_R(T, v_c) \simeq 21$, and $\langle \mu \rangle_R(T, v_c) \simeq 4900$. These values confirm that the system is in regime SNL.

As expected from section 2.3, once the plateau regime has been reached (see figures 4 and 5) the time dependence of the amplitude spectrum is weak (see figure 6). Therefore, we may neglect this dependence and consider that the self-consistent dynamics can be approximated by the non-self-consistent one, generated by (9). Indeed when the distribution function has reached the plateau shape both in velocity and in position, the Fourier coefficients in (16) are almost zero (because f is constant), bringing time variation of the waves to rest: the Vlasov equation lands on the non-self-consistent configuration. The works on Hamiltonian chaotic dynamics (9), recalled in the introduction and more precisely in appendix A, show that QL estimates hold if the wave spectrum satisfies two sufficient assumptions.

The first one requires the wave amplitude spectrum not to have holes larger than the order of a width Δv_D . From figure 7, we observe that the typical diffusion coefficient values are smooth enough with respect to their velocity (or wavenumber).

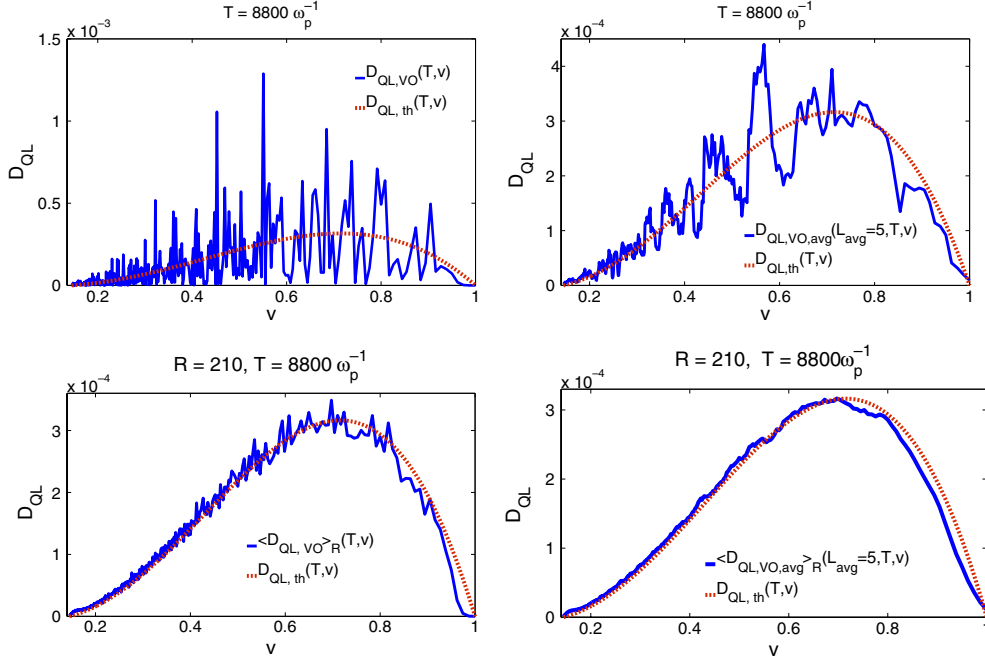


Figure 7. Quasilinear diffusion coefficient: (top) for a single realization; (bottom) ensemble averaged over $R = 210$ simulations; (left) for each velocity from the wave intensity; (right) averaged over $2L + 1 = 11$ neighbouring waves. Dashed red lines: theoretical QL prediction (4).

Even if nearby waves seem to have strongly inhomogeneous amplitude values (see [8]), and related diffusion coefficients, with respect to velocity in figure 7 (top left), once averaged over a velocity width corresponding to a floating average (29) with $L_{\text{avg}} = 5$, wave amplitudes and diffusion coefficients appear smooth with respect to velocity in figure 7 (bottom right). Yet our floating average is very conservative: it should really be performed with the v -dependent range $L_{\text{avg,D}}(t, v) = \Delta v_D / \Delta v_\varphi = \tau_{\text{discr}} / \tau_D = \mathcal{B}^{-1}$, which is about 22 near the middle of the wave spectrum (see figures 8). Therefore the first requirement, namely the absence of holes larger than the order of a width Δv_D , is satisfied.

The second requirement on the wave spectrum is randomness of the final phase. Figure 9 (left) shows the phases at $t = 10^4 \omega_p^{-1}$ for a single, typical run, with random initial phases uniformly distributed on the circle: the wave evolution does not generate strong phase correlations between waves, and waves with neighbouring velocities have quite independent phases. In figure 9 (right) the histograms of the phases show that the final phases appear to be drawn independently from a uniform distribution on the circle as was the case at initial time. Therefore, the numerical wave spectrum fulfils the conditions leading to QL estimates.

Finally, we assess the validity of the QL diffusive model for particle motion in the plateau regime, by observing the spreading of $N = 20$ test particles for each of the $R = 210$ realizations of the wave complex envelopes $\zeta_m(t_0)$ at $t_0 = 8800 \omega_p^{-1}$. These particle motions are obtained by direct integration of their equations of motion (11)–(12) with fixed ζ_m , using a reversible symplectic second order code. The resulting statistics are displayed in terms of the even moments of the ‘test’ particles released at t_0 with velocity $v_c = (u_0 + u_1)/2$ at independent (uniformly distributed) random positions in the wave spectrum; an estimate for the numerical accuracy of the test particle motion is provided by the standard deviations of the moments.

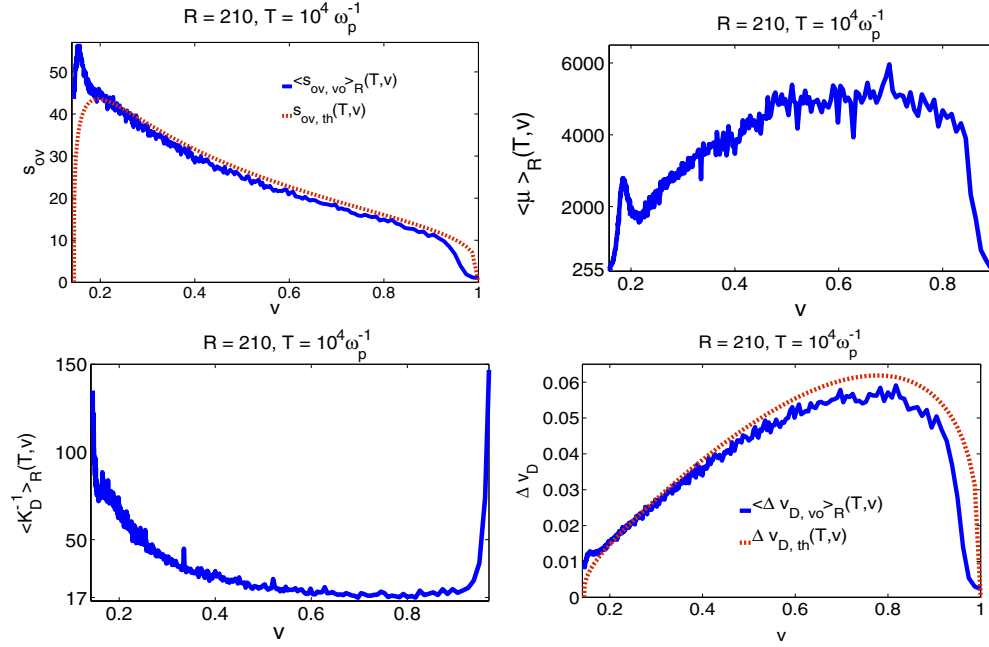


Figure 8. Physical parameters, compared with their theoretical estimates from (4): overlap parameter s_{ov} , time scale ratio μ , reciprocal Kubo number K_D^{-1} and diffusion width Δv_D .

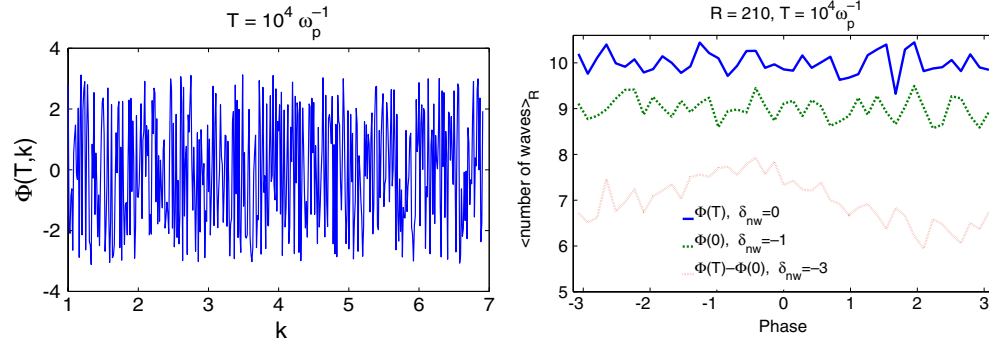


Figure 9. (Left) typical final phase of the wave spectrum for a single realization. (Right) histograms of the wave phases: initial phase (dashed green line, shifted downwards by $\delta_{nw} = -1$), final phase (continuous blue line), and difference of initial and final phases (dotted red line, shifted downwards by $\delta_{nw} = -3$). (Colour online.)

In figure 10 these moments are compared with those of the solution to the Fokker-Planck equation (1) for velocity diffusion, using the velocity-dependent diffusion constant D_{QL} displayed in figure 7 (top), with initial data a Dirac distribution at velocity v_c . To allow for direct observation of the velocity distribution departure from Gaussianity, we plot the moment roots $(|\Delta v(t)|^{2k}/(1 \cdot 3 \dots (2k-1)))^{1/k}$, which would coincide with the second moment if the distribution were Gaussian [21]. In these figures, time is normalized with the discretization time τ_{discr} associated with velocity v_c , and $\Delta v(t)$ is normalized so that, for pure diffusion over an infinite domain with constant D_{QL} , all plots would condense to a single straight line with

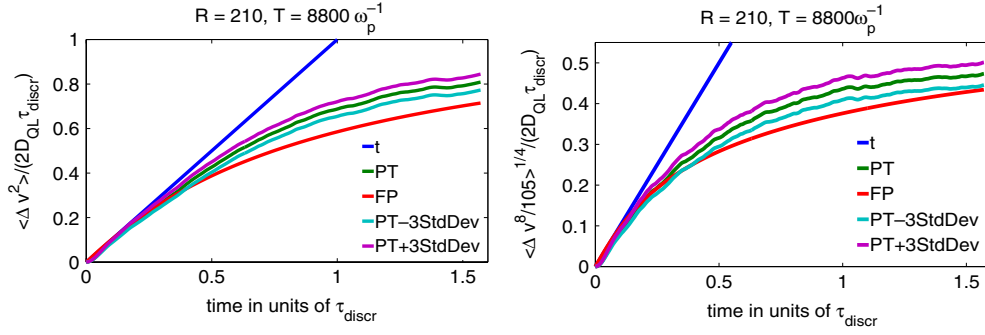


Figure 10. Scaled moments of orders 2 and 8 of the particle velocity deviation. FP: Fokker–Planck equation. PT: motion of 20 test particles in $R = 210$ realizations of the wave complex amplitudes $\zeta_m(T)$. (Colour online.)

unit slope. The figures display $k = 1$ (variance) and $k = 4$ (corresponding to eighth moment); other values ($k = 2, 3$) are very similar as can be seen in [8].

We may consider the agreement with QL predictions as satisfactory, given that there is no adjustable parameter in the modelling and that the spreading width (over which the diffusion approximation is expected to hold possibly) is not very small in comparison with the total wave spectrum width Δv_{spec} : indeed the drawback of the large ratio $\Delta v_D / \Delta v_\varphi = \tau_{discr} / \tau_D = \mathcal{B}^{-1}$ (for the given ratio $\Delta v_{spec} / \Delta v_\varphi$ of the wave spectrum) is that diffusing particles may reach the plateau boundary soon, ceasing then to contribute to the growth of the moments, and undergo there (influenced by KAM-like boundaries) a motion which may depart from the diffusive QL approximation further than near the centre of the plateau. There is thus no compelling indication for rejecting the simple QL model (1), with coefficient $D_{QL}(v)$, when describing particle transport in the plateau regime of the full Vlasov-waves system.

5. Triangular case

In this section we consider a triangular initial distribution function f_0 , which has the advantage of yielding more easily a large number of spreading widths Δv_D over the plateau width Δv_{spec} , at the expense of a larger computation time though. We performed fewer runs ($R = 13$) and discuss them here to stress the genericity of the behaviour observed above in the saturation regime.

The triangle vertices are $(u_0, 0)$, $(u_1, 2/\Delta v_{spec})$ and $(u_1, 0)$, defining the initial distribution $f_0(v) = 2(v - u_0) / \Delta v_{spec}^2$ for all $v \in [u_0, u_1]$ and 0 elsewhere. Momentum conservation yields

$$\mathfrak{P}_w^\infty - \mathfrak{P}_w^0 = \frac{\Delta v_{spec}}{6}. \quad (30)$$

We choose an initial wave spectrum ($\{|\zeta_m|\}, \{\varphi_m\}$) such that the wave amplitude $|\zeta_m|$ is given by (27) with

$$\psi_\infty(v) = \int_{u_0}^v (f_\infty(\xi) - f_0(\xi)) d\xi = \frac{(u_1 - v)(v - u_0)}{(u_1 - u_0)^2} \quad (31)$$

and phases φ_m are given by independent uniformly distributed random variables on the real circle. The physical parameters of the simulations are $\omega_p = 1$, $v_0 = 200$, $M = 1200$, $\eta = 10^{-5}$, $T_{end} = 9 \times 10^5$ ($\simeq 2 \max\{\langle \gamma_L(0) \rangle^{-1}, T_{dif}\}$), $L_x = 402 \pi$, $v_{min} = 0.09$ and $v_{max} = 1.1$. The numerical parameters of the simulations are $N_x = 5632$ ($n_{\delta x} \simeq 4$), $N_v = 1408$ ($n_{\Delta v_\varphi} \simeq 1$),

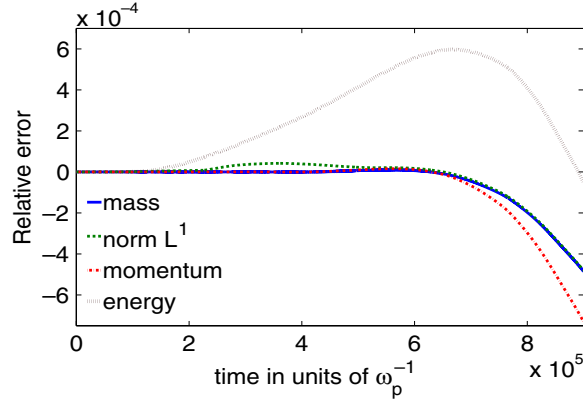


Figure 11. Relative error in conservation laws. The error in mass is almost equal to the L^1 error, so that these lines superpose in the figure. (Colour online.)

$\Delta t = 0.25$ ($n_\phi \simeq 4$) and $\epsilon_{\zeta^0} = \exp(-4.5)$. The coarse *a priori* estimates of section 3.4 yield for the plateau $K_D^{-1} \simeq 144$, $s_{\text{ov}} \simeq 32$ (or $B^{-1} \simeq 20$) and $\Delta v_D \simeq 6.1 \times 10^{-3}$. Finally we have $u_0 = 0.144$, $u_1 = 1$, $k_{\text{min}} = 1$, $k_{\text{max}} = 6.97$ and $1/(u_1 - u_0) = 1.17$.

5.1. Validation of the linear and nonlinear regimes

We first validate the code in the linear and nonlinear regimes. Figure 11 shows that the mass and the L^1 -norm (indistinguishable in the figure) are conserved with a relative error less than 0.05% up to time $9 \times 10^5 \omega_p^{-1}$. Total momentum and energy are well preserved, respectively, with relative error less than 0.08% and 0.06% up to the final time $9 \times 10^5 \omega_p^{-1}$. The evolution of the distribution of the momentum and energy between wave, particle and coupling terms is similar to the hyperbolic case (see [8]), ending with a global momentum transfer from particles to waves about 1/5 of the total momentum (which is of the order of QL estimate (30)) while energy transfer is about a quarter of the total energy. Wave–particle coupling energy remains negligible, which supports again the strong randomness picture of the microscopic dynamics in the nonlinear regimes.

Since the initial distribution function is affine in velocity, the Landau growth rate of the waves varies quadratically with the velocity. From figure 12 (left), we observe a first regime from time $t = 0$ to $t = 1250 \omega_p^{-1}$ where the logarithm of the waves' total energy appears to vary linearly with time. More significantly, as the growth rates depend on velocity, figure 12 (right) indicates a linear stage, where every wave m grows exponentially with its prescribed rate, up to time $t = 1250 \omega_p^{-1}$.

We next observe a second regime for time $t > 1250 \omega_p^{-1}$, where the faster waves no longer grow at the initial Landau rate, which indicates mode-coupling processes (INL regime), followed by a nonlinear saturation regime from time $t = 1.5 \times 10^5 \omega_p^{-1}$ to time $t = 9 \times 10^5 \omega_p^{-1}$ at which the plateau regime is settled (see figures 12 and 13).

5.2. Transition from stochastic to chaotic diffusion

In figure 13 (left) we observe that the space-averaged distribution function evolves from the triangular shape to the plateau one between times $t = 5.4 \times 10^4 \omega_p^{-1}$ and $t = 9 \times 10^5 \omega_p^{-1}$. Simultaneously, during the same time period, the growth rates of the waves fall from a strictly

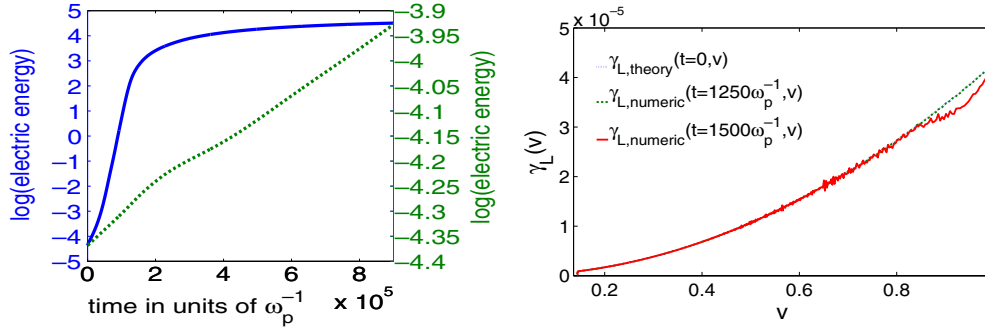


Figure 12. (Left) total electric energy (left axis, continuous blue line) for full simulation duration, and zoom (right axis, dotted green line) on initial evolution with $t_{\text{zoom}} = t/60$, i.e. with a time (horizontal) axis running from 0 to $15000\omega_p^{-1}$. (Right) growth rates of waves in linear (data for $t = 0$, $t = 1250\omega_p^{-1}$ appear almost superposed) and INL ($t = 1500\omega_p^{-1}$) regimes. (Colour online.)

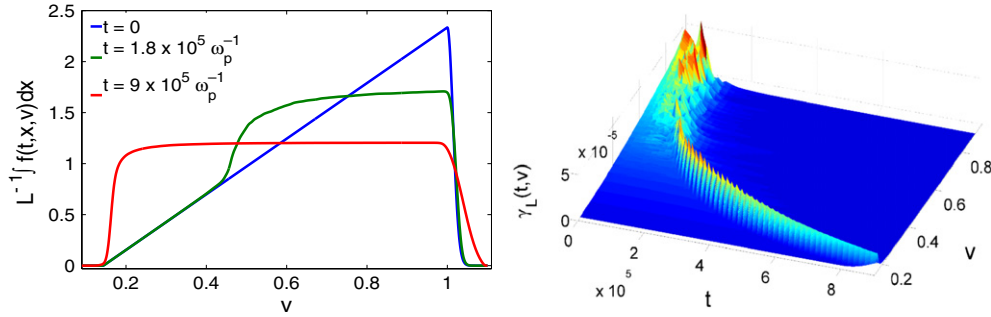


Figure 13. Time evolution of the space-averaged distribution function and of the corresponding Landau growth rate. (Colour online.)

positive value to a null one (see figure 13 (right)). In contrast to the hyperbolic case where the saturation of all waves and the vanishing of their growth rate γ occurred around the same time, here we observe the propagation of a front going from high velocity values to smaller ones. This front displays a hyperbolic-like profile in time (see figure 13 (right)), due to the v^2 variation of γ_L , making slower waves grow more slowly. The plateau regime is well settled at time $t = 9 \times 10^5 \omega_p^{-1}$.

For this triangular initial profile, the self-consistent wave spectrum is obtained by averaging over 13 realizations of the same Vlasov-wave test case where random initial phases are drawn independently from a uniform distribution on the circle. From figure 14, in the plateau regime, we observe rather good agreement of the QL prediction for the wave intensity spectrum (31) and for the diffusion coefficient with the ones obtained by self-consistent simulations of the Vlasov-wave model. These results yield again some support in favour of the validity of the QL theory. The relative lack of accuracy of results presented in figure 14 (bottom left) is due to our rough statistics with only 13 realizations. However figure 14 (bottom right) suggests what would appear if we considered a larger statistical ensemble.

In order to assess whether regime SNL, where strong chaotic diffusion holds, has been reached at the end of the simulation, we measure the parameters K_D , s_{ov} (or B^{-1}) and μ . From figure 15 we notice that at the middle of the phase velocity range of the wave spectrum, i.e. for $v_c = (u_0 + u_1)/2 \simeq 0.57$, and at time $T = 9 \times 10^5 \omega_p^{-1}$ in the plateau

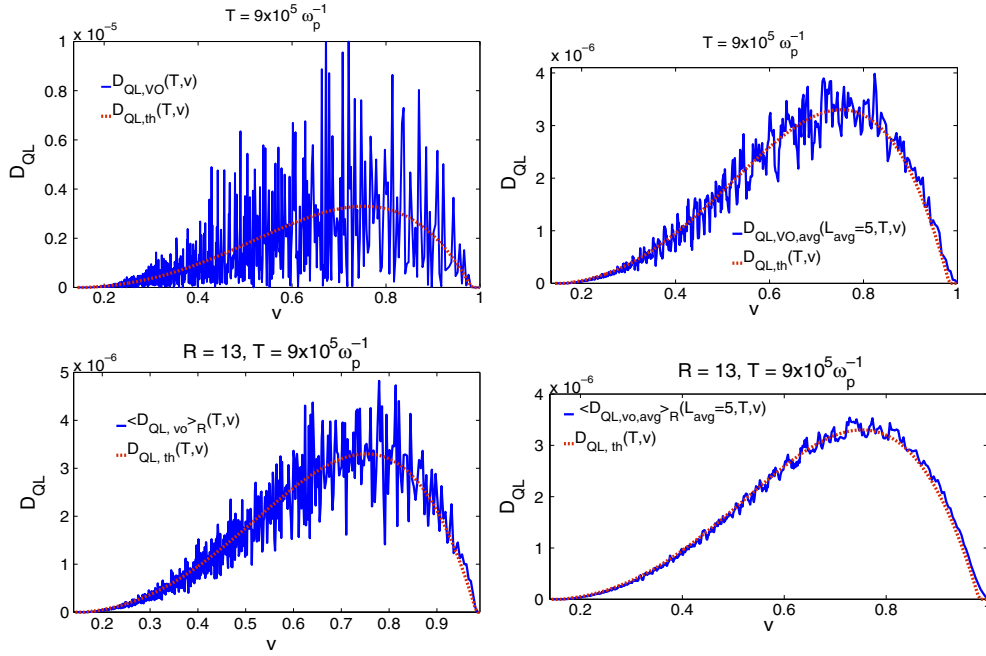


Figure 14. QL diffusion coefficient. (Top) typical coefficient for one realization; (bottom) ensemble average for $R = 13$ realizations; (left) value at each wave phase velocity; (right) average over $2L + 1 = 11$ neighbouring waves. Smooth line: coefficient predicted from (4).

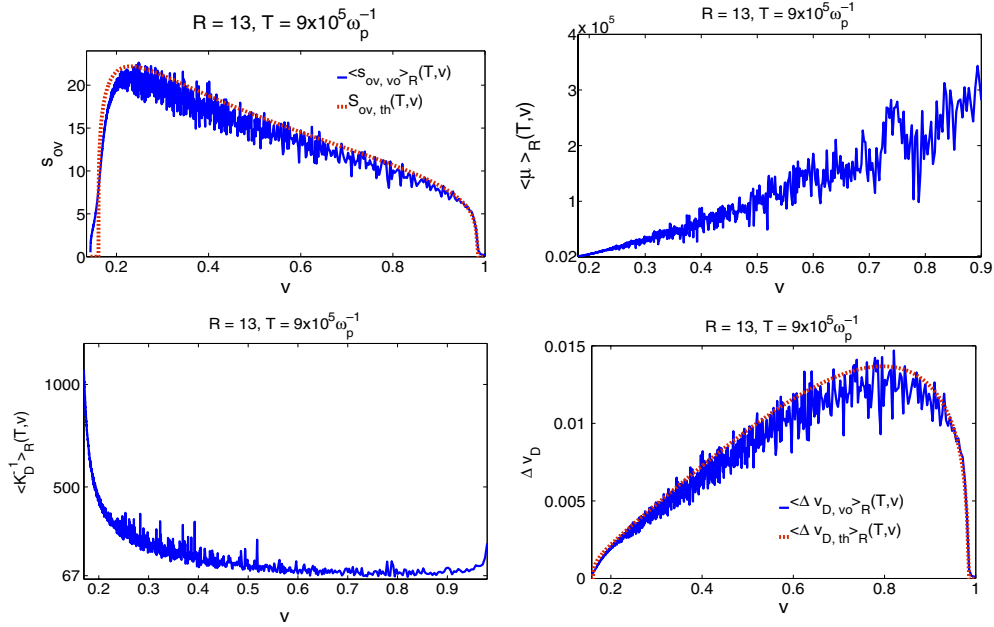


Figure 15. Physical parameters in the plateau regime.

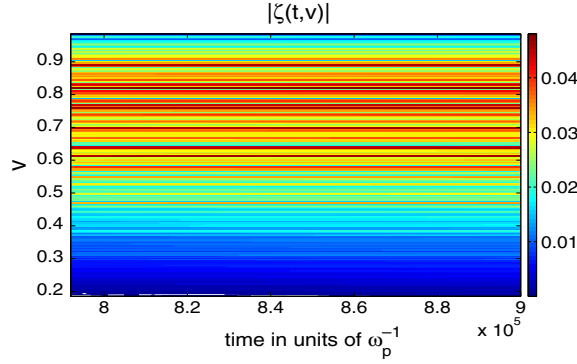


Figure 16. Time evolution of wave amplitudes $|\zeta(t, v)|$, from time $t_1 = 8 \times 10^5 \omega_p^{-1}$ to $t_2 = 9 \times 10^5 \omega_p^{-1}$ for a single realization. (Colour online.)

regime, we have $\langle s_{\text{ov}} \rangle_R(T, v_c) \simeq 15$, $\langle K_D^{-1} \rangle_R(T, v_c) \simeq 112$, $\langle \mu \rangle_R(T, v_c) \simeq 1.16 \times 10^5$ and $\langle \Delta v_D \rangle_R(T, v_c) \simeq 10^{-2}$ which corresponds to a range of wave velocities about 100 times as wide as the velocity diffusion width. These parameter values confirm that the system is in regime SNL of strong chaotic diffusion.

Since the plateau regime is well settled at time $t = 9 \times 10^5 \omega_p^{-1}$ (see figure 13), the amplitude spectrum variations are sufficiently small and thus negligible (see figure 16). We may again consider that the self-consistent dynamics can be approximated by the non-self-consistent one. In order that QL estimates should hold in regime SNL, the wave spectrum has to be smooth enough over the Dupree width, and the phases should be random. In figure 14 (top left) we observe for a single realization that the velocity dependence of the diffusion coefficient is very noisy, but when averaged over a velocity width corresponding to a floating average (29) with $L_{\text{avg}} = 5$, diffusion coefficients (and wave spectra alike) describe a smooth function with respect to velocity, see the right side of the figure. This is a conservative test, as at the middle of the phase velocity range of the wave spectrum, the ratio $L_{\text{avg,D}}(t, v) = \Delta v_D / \Delta v_\varphi = \mathcal{B}^{-1}$ is about 12 (see figure 15). Figure 14 shows that the average diffusion coefficients are quite smooth with respect to the velocity. The spectrum generated by our self-consistent simulations thus fulfils the first hypothesis about the absence of holes larger than the order of a width Δv_D .

From figure 17 (right) we observe that the final phases are drawn independently from a uniform distribution on the circle as was the case at initial time, which satisfies the second requirement. Even for a single, typical run, with random initial phases uniformly distributed on the circle, figure 17 (left) shows roughly that the final phases of waves with nearby velocities are uncorrelated. Therefore, the wave spectrum fulfils the assumptions which lead to QL estimates [22].

Again we test the validity of the QL diffusion model by directly integrating the particle equations of motion. We follow $N = 100$ test particles in $R = 13$ realizations of the wave data (ζ_m) at $T = 9 \times 10^5 \omega_p^{-1}$ and compare even moments of their velocity distribution with the corresponding moments of the solution to the Fokker–Planck equation with QL diffusion coefficient. Figure 18 shows that the agreement is very good up to times exceeding the discretization time τ_{discr} . This is much longer than for the hyperbolic initial particle velocity distribution, clearly thanks to the wave spectrum here allowing for more waves to act incoherently on the particles. The Fokker–Planck equation (1) definitely accounts for the motion of particles in the plateau wave spectrum.

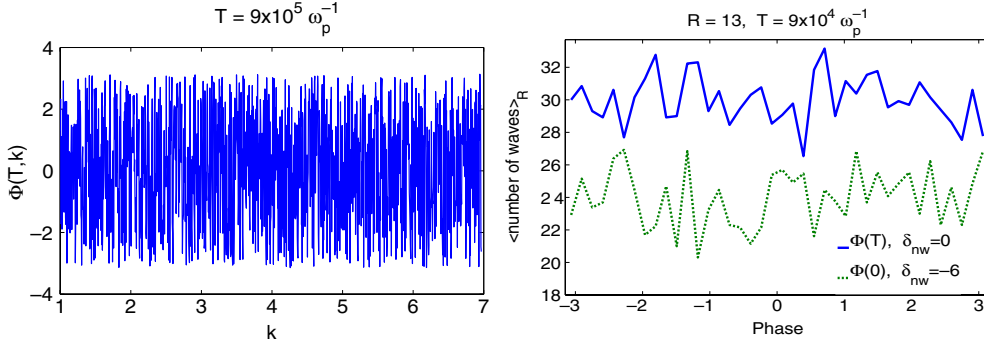


Figure 17. (Left) typical final phase of the wave spectrum for a single realization. (Right) histograms of the distribution of waves phases at initial time (dashed green line, shifted downwards by $\delta_{nw} = -6$) and final time (continuous blue line).

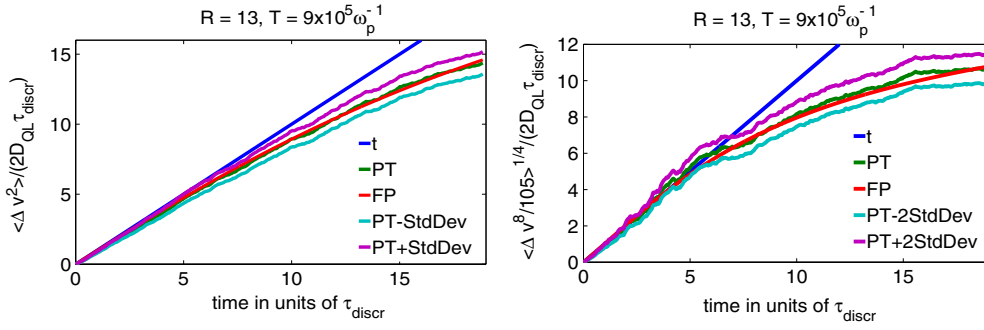


Figure 18. Even moments (scaled) of the particle velocity deviation. FP: Fokker–Planck equation. PT: motion of 100 test particles in $R = 13$ realizations of the wave amplitudes. (Colour online.)

6. Conclusion

The validity of quasilinear theory for describing the weak warm beam–plasma instability in the chaotic saturation regime was considered in this work both analytically and numerically. It was shown intuitively and analytically that there is no mode coupling in the saturation regime of the instability, where a plateau is present in the tail of the particle distribution function. This contradicts previous analytical works attempting to prove the validity of quasilinear theory in the strongly nonlinear regime of the weak warm beam–plasma instability [22, 29, 43, 44] and the ‘turbulent trapping’ ansatz aiming for the contrary [41].

Then this work described a series of self-consistent simulations of the weak warm beam–plasma instability within the Vlasov–wave description. They confirmed the occurrence of an enhanced growth rate in the intermediate nonlinear regime already shown in [16], and consistent with the perturbative calculation of [39]. This enhancement contradicts the analytical arguments for validity of quasilinear theory in [52]. However, the wave growth rate was shown to relax towards its quasilinear value when going into regime SNL. They also showed that QL theory remains valid in the strong chaotic diffusion regime (regime SNL). In particular, the QL diffusive approximation for particle motion in the saturated wave spectrum was shown to hold over time scales up to the order of the beam spreading through the wave spectrum. This work also confirmed the relevance of the diffusive model for particle motion in regime SNL by comparing the statistics of direct integration of the equations of motion with

the statistics of the diffusion model. Thus both the mode growth rates in regime INL and the particle diffusion process in the plateau regime SNL remain rather close to the QL predictions.

In conclusion, the main argument for a possible renormalization of the quasilinear growth rate and diffusion coefficient in the strongly nonlinear regime of the weak warm beam–plasma instability was discarded on an analytical and intuitive basis, and a thorough numerical simulation was consistent with the quasilinear prediction in this regime. Together with the refutation of other analytical works, this is an important milestone to the quasilinear controversy. However, a rigorous and intuitive description of the whole situation is still awaited.

Acknowledgments

This work was granted access to the high performance computing resources of IDRIS (IBM-Power6 computer) under allocation i-2010-056002 made by GENCI (Grand Equipement National de Calcul Intensif). It is a pleasure to acknowledge D Bénisti's comments, which were an incentive for revisiting the analytical part of the paper. YE is grateful to N Dubuit for technical tips.

Appendix A. Time scales for diffusion and velocity resonance boxes

This appendix makes more precise the discussion in section 1 about diffusive transport in the dynamics defined by Hamiltonian (9). Physically, the greater the velocity of a particle in a wave frame, the smaller the influence of the wave on the particle. Even in the chaotic regime, strong enough non-resonant waves may be treated through perturbation theory [4–6, 22]. Put briefly, the interaction is local in velocity.

This idea of locality was already present in the resonance-broadening concept introduced by Dupree [18]. A more complete analysis [4–6, 22] shows that for strong resonance overlap ($s_{\text{ov}} \gg 1$ or $\mathcal{B} \ll 1$), only waves with a phase velocity within the range (called resonance box) centred on the particle velocity of width $2\Delta v_{\text{box}}$ with $\Delta v_{\text{box}} \simeq 4.6\Delta v_{\text{D}}$ contribute to chaotic transport of the particle. Note that parameter \mathcal{B} can be rewritten as the ratio $\mathcal{B} = 4.6\Delta v_{\varphi}/\Delta v_{\text{box}}$, so that $4.6\mathcal{B}^{-1}$ can be viewed as the typical number of waves in a resonance box. We can also introduce the parameter $K_{\text{box}} = \Delta v_{\text{box}}/\Delta v_{\text{spec}}$ which is equivalent to the Kubo number K_{D} and is associated with the competition between stochastic and deterministic time scales in stochastic processes. Finally we can introduce the time $\tau_{\text{box}} = (2\Delta v_{\text{box}})^2/(2D_{\text{QL}}) \simeq 11\tau_{\text{spread}} \simeq 40\tau_{\text{D}}$ which is the typical time it takes for a resonant particle to wander through a resonance box.

Since large-scale chaos makes the orbit unconfined in velocity, it visits a sequence of resonance boxes of width $2\Delta v_{\text{box}}$, where the wave random phases are independent. Hence, the velocity undergoes a series of independent increments, which lead to diffusion by a central limit effect. Therefore if we note $N_{\text{box}} = \Delta v_{\text{spec}}/(2\Delta v_{\text{box}}) \simeq (9K_{\text{D}})^{-1}$, we see that the regime of strong chaotic diffusion, regime SNL, is in fact characterized by the conditions $\mu \gg 1$ (slow wave evolution), $\mathcal{B} \ll 1$ (strong chaos by strong resonance overlap) and $N_{\text{box}} \gtrsim 3$ (wide diffusion range). It is also important to note that a random initial position alone does not impose Gaussian statistics on the velocity: wave phase randomness is essential [4–6, 22].

The wave phase randomness of course underlies the original QL theory, as it essentially implies that, for short times, the particle is subject to an uncorrelated force field, physically a white noise. Considering this picture as a perturbation to ballistic motion of the particle leads first to the traditional requirement $\langle k^2 \Delta x^2 \rangle \lesssim 4\pi^2$ of the original QL estimates, which applies only for $t \lesssim \tau_{\text{spread}}$ and forces the orbit to have a weak dependence on all $M \gg 2$ phases simultaneously. However, if the orbit merely has a weak dependence on any $N_{\varphi} = 2$ phase, all

other phases being fixed (which is less stringent than the previous condition of type $N_\varphi = M$), formal integration of the equation of motion reveals that $\langle \Delta v^2 \rangle$ takes its QL value over times beyond τ_{spread} [4–6, 22], as is recalled now.

Actually, linear theory enables one to compute rigorously the small variation of the orbit when any two phases are varied [22, 28–30]. Indeed, since the particle initial position is the same for all realizations of the wave phases, the initial mismatch between two realizations of the orbit is initially small and can also be computed by linear theory. This calculation shows that $D = D_{\text{QL}}$ for $t \lesssim \tau_{\text{QL}} = \tau_{\text{spread}} |\ln \mathcal{B}|$ for strong resonance overlap (and in particular for a continuous spectrum $\mathcal{B} \rightarrow 0$). In this regime, $\tau_{\text{QL}} \gg \tau_{\text{spread}}$, which means that the QL estimate for the diffusion coefficient is correct for times much larger than τ_{spread} . Moreover as $\tau_{\text{QL}} \gg \tau_{\text{box}} \gtrsim \tau_{\text{spread}}$ for $\mathcal{B} \ll 1$, there is an overlap between the initial non-chaotic QL regime and the final chaotic diffusion one. This confirms that a small value of \mathcal{B} (strong resonance overlap) is required for the transition from regime L to regime SNL.

The time scale over which QL estimates hold can still be stretched significantly using a different viewpoint. Indeed, if the waves are random, their superposition is essentially an approximation to white noise for times $t > \tau_{\text{ac}} \sim (k \Delta v_{\text{spec}})^{-1}$. However, this white noise is approximated using a discrete wave spectrum, which allows for echo at a period $2\pi \tau_{\text{discr}} = 2\pi / (k \Delta v_\varphi)$. Therefore, one can also prove that for a time span $0 < t \lesssim \tau_{\text{discr}}$ the particle velocity essentially undergoes Brownian diffusion. For longer times, the strong overlap limit $\mathcal{B} \rightarrow 0$ implies that the particle motion ‘forgets’ its initial sampling of the wave spectrum, which enables one to prove the validity of QL estimates for large t/τ_{discr} through an ergodic theorem using martingale properties of the dynamics [20, 21, 24].

Appendix B. Mode–mode coupling in the wide plateau regime

In this appendix we calculate the modulation of the particle velocity near the plateau edge and the resulting feedback on waves, considered in section 2.2. This problem can be treated perturbatively, as the edge particles move quite regularly, with velocity $v(t) > v_b$ or $v(t) < v_a$, and are coupled to waves with phase velocity $v_\varphi \in [u_0, u_1] \subset [v_a, v_b]$. Therefore, the particles stay away from resonances; typically one finds this $\Delta v_{\text{edge}} \approx v_b - u_1 \sim (\varepsilon \beta \zeta_*)^c$ with $c = \frac{1}{2}$ for a single wave model and $c = \frac{2}{3}$ for a resonance box scaling [5].

The water bag distribution, with height f_0 , is fully described by its two boundaries, where by assumption the particles move regularly with velocities near v_0 and v_1 . The M waves modulate these boundaries, so that at time t their equations read $v = v_-(t, x) = v_0 + \delta v_-(t, x)$ and $v = v_+(t, x) = v_1 + \delta v_+(t, x)$. Here x is a mere label on the position axis, and $f_0 = 1/(v_1 - v_0)$. The wave deformation $\theta_m = \zeta_m(t) - \zeta_m(0)$, which must be small over the time scale of interest, is generated by

$$\begin{aligned} \dot{\theta}_m(t) &= \varepsilon i \frac{\beta_m}{k_m L} \int_0^L \int_{v_0 + \delta v_-(t, x)}^{v_1 + \delta v_+(t, x)} e^{-ik_m x + i\omega_m t} f_0 \, dv \, dx \\ &= \varepsilon i \frac{\beta_m}{k_m L} \int_0^L \frac{v_1 + \delta v_+(t, x) - v_0 - \delta v_-(t, x)}{v_1 - v_0} e^{-ik_m x + i\omega_m t} \, dx \\ &= \varepsilon i \frac{\beta_m}{k_m L} \int_0^L \frac{\delta v_+(t, x) - \delta v_-(t, x)}{v_1 - v_0} e^{-ik_m x + i\omega_m t} \, dx \end{aligned} \quad (\text{B.1})$$

which is $\mathcal{O}(\varepsilon \beta_m k_m^{-1} L^{-1} \int_0^L (|\delta v_+| + |\delta v_-|) dx / \Delta v_{\text{plat}})$. The dominant contribution to (B.1) in an ε expansion is thus determined by the lowest order approximation to the k_m Fourier mode of the modulations $\delta v_\pm(t, x)$, which we now estimate.

Since particles on the boundaries follow characteristics of the Vlasov equation, we now describe the faster boundary in terms of particle positions x_0 at time t_0 . We compute the correction $s(t) = x(t) - x_0 - v_1 t$, $w(t) = v(t) - v_1$ by integrating the characteristic equations in the form

$$\dot{s} = w, \quad (\text{B.2})$$

$$\dot{w} = \text{Re} \sum_m i \varepsilon \beta_m \zeta_m(t) e^{i(k_m x - \omega_m t)} \quad (\text{B.3})$$

$$= \sum_m \frac{i}{2} \varepsilon [\alpha_m e^{i(k_m s + \Omega_m t)} - \alpha_m^* e^{-i(k_m s + \Omega_m t)}] \quad (\text{B.4})$$

where $\Omega_m = k_m v_1 - \omega_m$ and $\alpha_m = \beta_m \zeta_m e^{ik_m x_0}$. To dominant order in ε , we may treat $\zeta_m(t)$ as a constant, ζ_m .

By the adiabatic assumption, s must be uniformly small over the time interval of interest, and we Taylor expand the exponentials with respect to $s(t) = \sum_{j=1}^3 \varepsilon^j s_j + \mathcal{O}(\varepsilon^4)$, so that

$$s_1(t) = S_1 + W_1 t - \sum_\ell \frac{i}{2} \Omega_\ell^{-2} (\alpha_\ell e^{i\Omega_\ell t} - \alpha_\ell^* e^{-i\Omega_\ell t}) \quad (\text{B.5})$$

where constants S_1 , W_1 are arbitrary. They depend on x_0 , but the KAM requirement for the boundary mean velocity being v_1 is met by letting both of them vanish ($W_1 = 0$ eliminates secular behaviour, and $S_1 = 0$ ensures that the boundary is labelled uniformly by x_0 , on average). This in turn leads to the second order approximation,

$$\ddot{s}_2 = \sum_p \frac{i}{2} [\alpha_p e^{i\Omega_p t} + \alpha_p^* e^{-i\Omega_p t}] i k_p s_1 \quad (\text{B.6})$$

so that

$$s_2(t) = S_2 + W_2 t + \sum_p \sum_\ell \frac{i}{4} \Omega_\ell^{-2} k_p [(1 - \delta_{\ell p})(\Omega_\ell - \Omega_p)^{-2} (\alpha_p^* \alpha_\ell e^{i(\Omega_\ell - \Omega_p)t} - \alpha_p \alpha_\ell^* e^{i(\Omega_p - \Omega_\ell)t}) + (\Omega_\ell + \Omega_p)^{-2} (\alpha_p \alpha_\ell e^{i(\Omega_\ell + \Omega_p)t} - \alpha_p^* \alpha_\ell^* e^{-i(\Omega_\ell + \Omega_p)t})] \quad (\text{B.7})$$

where again we set $W_2 = 0$, $S_2 = 0$, and $\delta_{\ell p}$ is the Kronecker symbol. The equation for the third order velocity correction follows

$$\dot{w}_3 = \sum_q \frac{i}{2} \left[\alpha_q e^{i\Omega_q t} \left(i k_q s_2 - \frac{1}{2} k_q^2 s_1^2 \right) + \alpha_q^* e^{-i\Omega_q t} \left(i k_q s_2 + \frac{1}{2} k_q^2 s_1^2 \right) \right]. \quad (\text{B.8})$$

Its solution, with $W_3 = 0$ as for the lower orders, reads

$$w_3 = \frac{1}{16} \sum_{q,p,\ell} k_q^2 \Omega_p^{-2} \Omega_\ell^{-2} (W_{qp\ell} + W_{q,-p,-\ell} + W_{-q,p,-\ell} + W_{-q,-p,\ell}) - \frac{1}{8} \sum_{q,p,\ell} k_q k_p \Omega_\ell^{-2} (\Omega_p + \Omega_\ell)^{-2} (W_{qp\ell} + W_{q,-p,-\ell}) - \frac{1}{8} \sum_{q,p,\ell} k_q k_p \Omega_\ell^{-2} (\Omega_p - \Omega_\ell)^{-2} (1 - \delta_{p\ell}) (W_{-q,p,-\ell} - W_{-q,-p,\ell}) \quad (\text{B.9})$$

where

$$\begin{aligned}
 W_{qp\ell} &= (\Omega_q + \Omega_p + \Omega_\ell)^{-1} (\alpha_q \alpha_p \alpha_\ell e^{i(\Omega_q + \Omega_p + \Omega_\ell)t} + \alpha_q^* \alpha_p^* \alpha_\ell^* e^{-i(\Omega_q + \Omega_p + \Omega_\ell)t}) \\
 W_{q,-p,-\ell} &= (\Omega_q - \Omega_p - \Omega_\ell)^{-1} (\alpha_q \alpha_p^* \alpha_\ell^* e^{i(\Omega_q - \Omega_p - \Omega_\ell)t} + \alpha_q^* \alpha_p \alpha_\ell e^{-i(\Omega_q - \Omega_p - \Omega_\ell)t}) \\
 W_{-q,p,-\ell} &= (-\Omega_q + \Omega_p - \Omega_\ell)^{-1} (\alpha_q^* \alpha_p \alpha_\ell^* e^{i(-\Omega_q + \Omega_p - \Omega_\ell)t} + \alpha_q \alpha_p^* \alpha_\ell e^{i(\Omega_q - \Omega_p + \Omega_\ell)t}) \\
 W_{-q,-p,\ell} &= (-\Omega_q - \Omega_p + \Omega_\ell)^{-1} (\alpha_q^* \alpha_p^* \alpha_\ell e^{i(-\Omega_q - \Omega_p + \Omega_\ell)t} + \alpha_q \alpha_p \alpha_\ell^* e^{i(\Omega_q + \Omega_p - \Omega_\ell)t}) \quad (\text{B.10})
 \end{aligned}$$

To compute the δv_+ contribution to (B.1) we only need the k_m spatial Fourier component in w , as $\delta v_+(t, x) = w(t, x_0) = w(t, x - v_1 t - s)$. Thus, to dominant order, $e^{-ik_m x} \delta v_+(t, x) = e^{-ik_m x_0 - ik_m v_1 t} w(t, x_0 - v_1 t) + \mathcal{O}(k_m s w)$, and in the integral this change of variable yields $dx = dx_0 + ds(x_0)$. The ds integral is $\mathcal{O}(\varepsilon)$ smaller than the dx_0 integral, hence it is negligible. Therefore, we estimate now

$$\begin{aligned}
 \sigma_m &= \varepsilon i \frac{\beta_m}{k_m L} \int_0^L \frac{\delta v_+(t, x)}{v_1 - v_0} e^{-ik_m x + i\omega_m t} dx \\
 &\simeq \varepsilon i \frac{\beta_m}{k_m L} \int_0^L \frac{w(t, x_0)}{v_1 - v_0} e^{-ik_m x_0 - i\Omega_m t} dx_0. \quad (\text{B.11})
 \end{aligned}$$

The space dependence of w , due to $\alpha_p = \beta_p \zeta_p e^{ik_p x_0}$, implies that w_1 contributes to σ_m only through the $\ell = m$ spatial component. This contribution $\sigma_{m,1} = \mathcal{O}(\varepsilon^2)$ does not oscillate as its time dependence fulfils the resonance condition $\Omega_\ell = \Omega_m$ because of the specific dispersion relation, $\omega_m = \omega_p$, $k_m = (m + v_0)2\pi L^{-1}$. However, it involves no other wave than m , and does not couple waves nonlinearly.

The w_2 contribution to σ_m oscillates in time, because some waves ℓ, p , meeting the spatial resonance condition $k_m = c_\ell k_\ell + c_p k_p$ (imposed by the space integral over x_0) for some $c_\ell, c_p \in \{-1, 1\}$, will verify $c_\ell \Omega_\ell + c_p \Omega_p = k_m v_1 - (c_\ell + c_p)\omega_p = \Omega_m + (1 - c_\ell - c_p)\omega_p$. Hence they cannot meet the time-resonance condition $\Omega_m = c_\ell \Omega_p + c_p \Omega_\ell$.

Most terms in w_3 also generate time-oscillating terms in σ_m , but some waves ℓ, p, q do fulfil the non-oscillation condition $\Omega_m = \Omega_p + \Omega_q - \Omega_\ell$, and these triplets automatically meet the spatial resonance condition $k_m = k_p + k_q - k_\ell$. These four-wave coupling terms occur in a degenerate form, as any pair $p, q \in \mathbb{Z}$ defines a resonant partner $\ell = p + q - m$. The four-wave coupling terms in σ add up to

$$\sigma_m^{\text{res}} = \frac{\varepsilon^4 \beta_m}{16k_m(v_1 - v_0)} \sum_{p,q,\ell} \beta_p \beta_q \beta_\ell C_{pq} \zeta_\ell^* \zeta_p \zeta_q \quad (\text{B.12})$$

with

$$\begin{aligned}
 C_{pq} &= -(k_\ell^2 \Omega_p^{-2} \Omega_q^{-2} + k_q^2 \Omega_\ell^{-2} \Omega_p^{-2} + k_p^2 \Omega_q^{-2} \Omega_\ell^{-2}) + 2k_\ell k_p \Omega_q^{-2} (\Omega_p + \Omega_q)^{-2} \\
 &\quad + 2(1 - \delta_{\ell p}) C'_{p\ell} k_q \quad (\text{B.13})
 \end{aligned}$$

where $\ell = p + q - m$ and

$$\begin{aligned}
 C'_{p\ell} &= (\Omega_\ell - \Omega_p)^{-2} (k_\ell \Omega_p^{-2} - k_p \Omega_\ell^{-2}) \\
 &= (\Omega_\ell - \Omega_p)^{-1} v_1^{-1} \Omega_\ell^{-2} \Omega_p^{-2} (\Omega_\ell^2 + \Omega_\ell \Omega_p + \Omega_p^2 + \Omega_p (\Omega_\ell + \Omega_p)). \quad (\text{B.14})
 \end{aligned}$$

In the four-wave coupling coefficient C_{pq} all terms are order unity in the limit of a dense spectrum, except those contributing to C'_{pq} . In the latter terms the worst divergence scales like $(\Omega_{p+1} - \Omega_p)^{-1} = L/(2\pi v_1)$, for $\ell = p \pm 1$, coupling waves with nearest wavenumbers (and nearly equal phase velocities). The other terms are milder, and the resulting, harmonic-like

truncated series with coefficients $(\Omega_{p+1} - \Omega_p)^{-1}$ will typically involve wave envelope factors $\zeta_\ell^* \zeta_p \zeta_q$ with incoherent phases, ensuring its convergence.

Therefore, with all k 's having comparable scales, the four-wave coupling term scales like a sum of $\varepsilon^4 \beta^4 |\zeta|^3 / [v_1(v_1 - v_0)\Omega_{\min}^2 \delta\Omega]$ and $\varepsilon^4 \beta^4 |\zeta|^3 k / [(v_1 - v_0)\Omega_{\min}^4]$. A similar argument applies to the slower boundary particles, with average velocity $v_0 > 0$.

Appendix C. Vlasov-wave semi-Lagrangian scheme

Let \mathcal{M}_h be a discretization of the μ -space (x, v) , with $N_x \times N_v$ mesh points with steps Δx and Δv , and f_h^n an approximation of f at time t^n on \mathcal{M}_h . The general algorithm to compute f_h^{n+1} for $t^{n+1} = t^n + \Delta t$ consists of three steps.

(1) Half time advection in physical space. This step consists in solving the equation

$$\partial_t f + v \partial_x f = 0, \quad t \in [t^n, t^{n+1/2}], \quad \text{with } f(t^n) = f_h^n. \quad (\text{C.1})$$

To solve (C.1) we integrate its associated characteristic curves' equation

$$\frac{dX}{dt}(t) = V(t)$$

on the time interval $[t^n, t^{n+1/2}]$ with $t^{n+1/2} = t^n + \Delta t/2$. We then get

$$X^n - X^{n+1/2} = \int_{t^{n+1/2}}^{t^n} V(t) dt = \int_{t^{n+1/2}}^{t^n} V(t^n) dt + \mathcal{O}(\Delta t^2) \simeq -V^n \Delta t/2,$$

where $(X^{n+1/2}, V^n) \in \mathcal{M}_h$ and X^n is the origin of the characteristic curve we look for. Therefore, the new distribution function f_h^* is such that

$$f_h^*(x, v) := \tilde{f}_h^{n+1/2}(X^{n+1/2}, V^n) = f_h^n(X^n, V^n), \quad \forall (x, v) \in \mathcal{M}_h.$$

As (X^n, V^n) is generally not in \mathcal{M}_h , it is interpolated using a B -spline.

(2) Time advection in velocity space. This step consists in solving the equation

$$\partial_t f + F(t, x, \{\zeta_m\}) \partial_v f = 0, \quad t \in [t^n, t^{n+1}], \quad \text{with } f(t^n) = f_h^*, \quad (\text{C.2})$$

where F is the factor of $\partial_v^0 f$ in (15). To solve (C.2) we integrate its characteristics equation (12), namely

$$\frac{dV}{dt}(t) = F(t, X(t), \{\zeta_m(t)\})$$

on the time interval $[t^n, t^{n+1}]$. We then get

$$\begin{aligned} V^{n+1} - V^n &= \int_{t^n}^{t^{n+1}} F(t, X(t), \{\zeta_m(t)\}) dt \\ &= \int_{t^n}^{t^{n+1}} F(t^{n+1/2}, X(t^{n+1/2}), \{\zeta_m(t^{n+1/2})\}) dt + \mathcal{O}(\Delta t^3) \\ &\simeq F(t^{n+1/2}, X^{n+1/2}, \{\zeta_m^{n+1/2}\}) \Delta t, \end{aligned}$$

where $(X^{n+1/2}, V^{n+1}) \in \mathcal{M}_h$ and V^n is the origin of the characteristic curve we look for. Therefore, the new distribution function f_h^{**} is such that

$$f_h^{**}(x, v) := \hat{f}_h^{n+1/2}(X^{n+1/2}, V^{n+1}) = f_h^*(X^{n+1/2}, V^n), \quad \forall (x, v) \in \mathcal{M}_h.$$

There remains to compute a ‘good’ approximation of $\{\zeta_m^{n+1/2}\}$, consistent with this step. To this purpose we integrate the wave equation (16) on the time interval $[t^n, t^{n+1}]$ and, using mid-point quadrature rule⁶, we obtain for all $m \in [1, M]$:

$$\begin{aligned} \zeta_m^{n+1/2} - \zeta_m^{n-1/2} &: = \zeta_m(t^{n+1/2}) - \zeta_m(t^{n-1/2}) \\ &= i\varepsilon \frac{\beta_m}{k_m} \frac{1}{L} \int_{t^{n-1/2}}^{t^{n+1/2}} \int_{\Lambda} e^{-i(k_m x - \omega_m t)} f(t, x, v) \, dv \, dx \, dt \\ &\simeq i\varepsilon \frac{\beta_m}{k_m} \Delta t \Delta v \frac{\Delta x}{L} e^{i\omega_m t^n} \sum_{q=1}^{N_x} \sum_{p=1}^{N_v} f(t^n, x_q, v_p) e^{-ik_m x_q} + \mathcal{O}(\Delta t^3) \\ &\simeq i\varepsilon \frac{\beta_m}{k_m} \Delta t \Delta v \frac{\Delta x}{L} e^{i\omega_m t^n} \sum_{q=1}^{N_x} \sum_{p=1}^{N_v} f_h^n(x_q, v_p) e^{-ik_m x_q} \\ &\simeq i\varepsilon \frac{\beta_m}{k_m} \Delta t e^{i\omega_m t^n} \frac{\Delta x}{L} \sum_{q=1}^{N_x} \rho_h^n(x_q) e^{-ik_m x_q} \simeq i\varepsilon \frac{\beta_m}{k_m} \Delta t e^{i\omega_m t^n} \mathcal{F}_h(\rho_h^n, k_m), \end{aligned}$$

where $\rho_h^n(\cdot) = \sum_{p=1}^{N_v} f_h^n(\cdot, v_p) \Delta v$ and $\mathcal{F}_h(\cdot, k)$ denotes the discrete Fourier transform at wave number k .

- (3) Half time advection in physical space. This step (formally identical to step 1) solves the equation

$$\partial_t f + v \partial_x f = 0 \quad t \in [t^{n+1/2}, t^{n+1}], \quad \text{with } f(t^{n+1/2}) = f_h^{**},$$

by convecting f along the characteristic, using

$$X^{n+1} - X^{n+1/2} = \int_{t^{n+1/2}}^{t^{n+1}} V(t) \, dt = \int_{t^{n+1/2}}^{t^{n+1}} V(t^{n+1}) \, dt + \mathcal{O}(\Delta t^2) \simeq V^{n+1} \Delta t / 2,$$

where $(X^{n+1}, V^{n+1}) \in \mathcal{M}_h$ and $X^{n+1/2}$ is the origin of the characteristic curve we look for. Therefore, the new distribution function is such that

$$f_h^{n+1}(x, v) = f_h^{n+1}(X^{n+1}, V^{n+1}) = f_h^{**}(X^{n+1/2}, V^{n+1}), \quad \forall (x, v) \in \mathcal{M}_h.$$

Putting together steps 1 and 3 shows that the time-discretized dynamics works in the classical leapfrog way where velocity is advanced at times t^n , while the position is advanced at times $t^{n+1/2}$. The algorithm is reversible within the accuracy of the spline interpolation (which prevents step 3 from being exactly the adjoint of step 1).

References

- [1] Adam J C, Laval G and Pesme D 1979 Reconsideration of quasilinear theory *Phys. Rev. Lett.* **43** 1671–5
- [2] Antoni M, Elskens Y and Escande D F 1998 Explicit reduction of N -body dynamics to self-consistent particle–wave interaction *Phys. Plasmas* **5** 841–52
- [3] Bechouche P and Besse N 2010 Analysis of a semi-Lagrangian method for the spherically symmetric Vlasov–Einstein system *ESAIM: M2AN* **44** 573–95
- [4] Bénisti D and Escande D F 1997 Origin of diffusion in Hamiltonian dynamics *Phys. Plasmas* **4** 1576–81
- [5] Bénisti D and Escande D F 1998 Finite range of large perturbations in Hamiltonian dynamics *J. Stat. Phys.* **92** 909–72
- [6] Bénisti D and Escande D F 1998 Nonstandard diffusion properties of the standard map *Phys. Rev. Lett.* **80** 4871–4

⁶ It is accurate to second order and a good approximation to a more expensive three-substeps fully symplectic integrator which would also require splitting (C.3) into three corresponding substeps.

- [7] Besse N 2004 Convergence of a semi-Lagrangian scheme for the one-dimensional Vlasov–Poisson system *SIAM J. Numer. Anal.* **42** 350–82
- [8] Besse N, Elskens Y, Escande D F and Bertrand P 2010 Validity of quasilinear theory: refutations and new numerical confirmation *Preprint HAL*: hal-00527149
- [9] Besse N and Mehrenberger M 2008 Convergence of classes of high-order semi-Lagrangian schemes for the Vlasov–Poisson system *Math. Comput.* **77** 93–123
- [10] Besse N 2008 Convergence of a high-order semi-Lagrangian scheme with propagation of gradients for the Vlasov–Poisson system *SIAM J. Numer. Anal.* **46** 639–70
- [11] Besse N and Sonnendrücker E 2003 Semi-Lagrangian schemes for the Vlasov equation on an unstructured mesh of phase space *J. Comput. Phys.* **191** 341–76
- [12] Boutros-Ghali T and Dupree T H 1981 Theory of two-point correlation function in Vlasov plasma *Phys. Fluids* **24** 1839–58
- [13] Cary J R, Doxas I, Escande D F and Verga A D 1992 Enhancement of the velocity diffusion in longitudinal plasma turbulence *Phys. Fluids B* **4** 2062–69
- [14] Cary J R, Escande D F and Verga A D 1990 Non quasilinear diffusion far from chaotic threshold *Phys. Rev. Lett.* **65** 3132–5
- [15] Cheng C Z and Knorr G 1976 The integration of the Vlasov equation in configuration space *J. Comput. Phys.* **22** 330–51
- [16] Doxas I and Cary J R 1997 Numerical observation of turbulence enhanced growth rates *Phys. Plasmas* **4** 2508–18
- [17] Drummond W E and Pines D 1962 Nonlinear stability of plasma oscillations *Nucl. Fusion Suppl.* **3** 1049–57
- [18] Dupree T H 1966 A perturbation theory for strong plasma oscillations *Phys. Fluids* **9** 1773–82
- [19] Dupree T H 1972 Theory of phase space density granulation in plasma *Phys. Fluids* **15** 334–44
- [20] Elskens Y 2007 Quasilinear limit for particle motion in a prescribed spectrum of random waves *Phys. AUC* **17** 109–21
- [21] Elskens Y 2010 Nonquasilinear evolution of particle velocity in incoherent waves with random amplitudes *Commun. Nonlinear Sci. Numer. Simul.* **15** 10–5
- [22] Elskens Y and Escande D 2003 *Microscopic Dynamics of Plasmas and Chaos* (Bristol: Institute of Physics Publishing)
- [23] Elskens Y and Firpo M-C 1998 Kinetic theory and large- N limit for wave–particle self-consistent interaction *Phys. Scr.* **T75** 169–72
- [24] Elskens Y and Pardoux E 2010 Diffusion limit for many particles in a periodic stochastic acceleration field *Ann. Appl. Prob.* **20** 2022–39
- [25] Escande D F 1989 Description of Landau damping and weak Langmuir turbulence through microscopic dynamics *Nonlinear World* vol 2, ed V G Bar'yakhtar *et al* (Singapore: World Scientific) pp 817–36
- [26] Escande D F 1991 Large scale structures in kinetic plasma turbulence *Large Scale Structures in Nonlinear Physics (Lecture Notes in Physics* vol 392) ed J D Fournier and P L Sulem (Berlin: Springer) pp 73–104
- [27] Escande D F 2010 Wave–particle interaction in plasmas: a qualitative approach *Long-Range Interacting Systems* ed T Dauxois *et al* (Oxford: Oxford University press) pp 817–36
- [28] Escande D and Elskens Y 2002 Quasilinear diffusion for the chaotic motion of a particle in a set of longitudinal waves *Acta Phys. Pol. B* **33** 1073–84
- [29] Escande D and Elskens Y 2002 Proof of quasilinear equations in the chaotic regime of the weak warm beam instability *Phys. Lett. A* **302** 110–9
- [30] Escande D and Elskens Y 2003 Proof of quasilinear equations in the strongly nonlinear regime of the weak warm beam instability *Phys. Plasmas* **10** 1588–94
- [31] Escande D and Elskens Y 2003 Microscopic dynamics of plasmas and chaos: the wave–particle interaction paradigm *Plasma Phys. Control. Fusion* **45** A115–24
- [32] Escande D and Elskens Y 2008 Self-consistency vanishes in the plateau regime of the bump-on-tail instability arXiv:0807.1839 [nlin.CD]
- [33] Feix M R and Bertrand P 2005 A universal model: the Vlasov equation *Transport Theory Stat. Phys.* **34** 7–62
- [34] Firpo M-C, Doveil F, Elskens Y, Bertrand P, Poleni M and Guyomarc'h D 2001 Long-time discrete particle effects versus kinetic theory in the self-consistent single-wave–particle interaction *Phys. Rev. E* **64** 026407
- [35] Firpo M-C and Elskens Y 1998 Kinetic theory of N -body description of wave–particle self-consistent interaction *J. Stat. Phys.* **93** 193–209
- [36] Galeev A A, Sagdeev R Z, Shapiro V D and Shevchenko V I 1980 Is renormalization necessary in the quasilinear theory of Langmuir oscillations? *Zh. Eksp. Teor. Fiz.* **79** 2167–74
Galeev A A, Sagdeev R Z, Shapiro V D and Shevchenko V I 1980 *Sov. Phys.—JETP* **52** 1095–9 (Engl. Transl.)
- [37] Hartmann D A, Driscoll C F, O'Neil T M and Shapiro V D 1995 Measurements of the warm beam instability *Phys. Plasmas* **2** 654–77

- [38] Landau L D 1946 On the vibrations of the electronic plasma *Zh. Eksp. Teor. Fiz.* **16** 574–86 reprinted in *Collected Papers of Landau* ed D ter Haar (Oxford: Pergamon, 1965) pp 445–60
- [39] Laval G and Pesme D 1983 Breakdown of quasilinear theory for incoherent 1-D Langmuir waves *Phys. Fluids* **26** 52–65
- [40] Laval G and Pesme D 1983 Inconsistency of quasilinear theory *Phys. Fluids* **26** 66–8
- [41] Laval G and Pesme D 1984 Self-consistency effects in quasilinear theory: a model for turbulent trapping *Phys. Rev. Lett.* **53** 270–3
- [42] Laval G and Pesme D 1999 Controversies about quasi-linear theory *Plasma Phys. Control. Fusion* **41** A239–46
- [43] Liang Y-M and Diamond P H 1993 Weak turbulence theory of Langmuir waves: a reconsideration of the validity of quasilinear theory *Comment. Plasma Phys. Control. Fusion* **15** 139–49
- [44] Liang Y-M and Diamond P H 1993 Revisiting the validity of quasilinear theory *Phys. Fluids B* **5** 4333–40
- [45] Malmberg J H and Wharton C B 1964 Collisionless damping of electrostatic plasma waves *Phys. Rev. Lett.* **13** 184–6
- [46] Mouhot C and Villani C 2009 On Landau damping arXiv:0904.2760
- [47] Mouhot C and Villani C 2010 Landau damping *J. Math. Phys.* **51** 015204
- [48] Mynick H E and Kaufman A N 1978 Soluble theory of nonlinear beam–plasma interaction *Phys. Fluids* **21** 653–63
- [49] O’Neil T M, Winfrey J H and Malmberg J H 1971 Nonlinear interaction of a small cold beam and a plasma *Phys. Fluids* **14** 1204–12
- [50] Onishchenko I N, Linetski A R, Matsiborko N G, Shapiro V D and Shevchenko V I 1970 Contribution to the nonlinear theory of excitation of a monochromatic plasma wave by an electron beam *ZhETF Pis. Red.* **12** 407–11
Onishchenko I N, Linetski A R, Matsiborko N G, Shapiro V D and Shevchenko V I 1970 *JETP Lett.* **12** 281–5 (Engl. Transl.)
- [51] Roberson C and Gentle K W 1971 Experimental test of the quasilinear theory of the gentle bump instability *Phys. Fluids* **14** 2462–9
- [52] Shapiro V D and Sagdeev R Z 1997 Nonlinear wave–particle interaction and conditions for applicability of quasilinear theory *Phys. Rep.* **283** 49–71
- [53] Spohn H 1991 *Large Scale Dynamics of Interacting Particles* (Berlin: Springer)
- [54] Tennyson J L, Meiss J D and Morrison P J 1994 Self-consistent chaos in the beam–plasma instability *Physica D* **71** 1–17
- [55] Tsunoda S I, Doveil F and Malmberg J H 1991 Experimental test of quasilinear theory *Phys. Fluids B* **3** 2747–57
- [56] Vedenov A A, Velikhov E P and Sagdeev R Z 1962 Quasilinear theory of plasma oscillations *Nucl. Fusion Suppl.* **2** 465–75